
SUPPORTING INFORMATION

Exploring the Tubular Self-assembly Landscape of Dinucleobase Amphiphiles in Water

Paula B. Chamorro,^a Fatima Aparicio,^{*a} Raquel Chamorro,^a Nerea Bilbao,^b Santiago Casado,^c
and David González-Rodríguez^{*a,d}

^a Organic Chemistry Department, Universidad Autónoma de Madrid, 28049 Madrid, Spain

^b Department of Chemistry, Division of Molecular Imaging and Photonics, KU Leuven, Celestijnenlaan 200F, B-3001 Leuven, Belgium.

^c IMDEA Nanociencia, c/Faraday 9, Campus de Cantoblanco, 28049, Madrid, Spain,

^d Institute for Advanced Research in Chemical Sciences (*IAdChem*), Universidad Autónoma de Madrid, 28049 Madrid

SUPPORTING INFORMATION

TABLE OF CONTENTS

SECTION	PAGE	
S0.	General Methods and Synthetic Procedures	S2
S1.	Preliminary Comparative Studies of the Aggregated States in Water	S17
S2.	Study of the effect of the Temperature on the Supramolecular Aggregation	S21
S3.	Study of the effect of the Solvent on the Supramolecular Aggregation	S29
S4.	Study of the effect of the pH on the Supramolecular Aggregation	S39

S0. General Methods and Synthetic Procedures

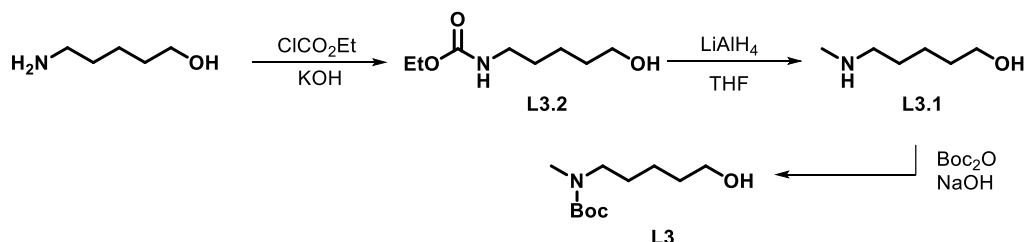
General Methods. Mass Spectrometry (MS) and High Resolution-Mass Spectrometry (HRMS). MALDI-TOF spectra were obtained from a BRUKER ULTRAFLEX III instrument equipped with a nitrogen laser operating at 337 nm. **NMR** spectra were recorded with a BRUKER AVANCE-II (300 MHz) instrument. The temperature was actively controlled at 298 K. Chemical shifts are measured in ppm using the signals of the deuterated solvent as the internal standard [CDCl_3 calibrated at 7.26 ppm (^1H) and 75.0 ppm (^{13}C) and THF-d_8 calibrated at 3.58 (^1H) and 25.5 ppm (^{13}C)]. **Column chromatography** was carried out on silica gel Merck-60 (230-400 mesh, 60 Å), and TLC on aluminium sheets precoated with silica gel 60 F254 (Merck). **UV/Vis spectra** were recorded with a JASCO V-660. **Emission spectra** were obtained with a JASCO-V8600. **CD** spectra were recorded with a JASCO V-815 equipment. Quartz cuvettes (1.0 / 0.1 cm path length) were used for the measurements. The slit width was set at 1000 μm and a DIT of 2 s was used. In all these last three instruments the temperature was controlled using a JASCO Peltier thermostatted cell holder with a range of 263–383 K, adjustable temperature slope, and accuracy of ± 0.1 K. **Transmission electron microscopy (TEM)** microscopy images were measured in a JEOL JEM 1400 PLUS working at an accelerating voltage of 40 to 120 kV at CNME in UCM. **Atomic Force Microscopy (AFM)** microscopy images were measured on a JPK NanoWizard II at IMdea Nanociencia and a *multimode* Nanoscope III A (Bruker), working in tapping mode at CNME in UCM. The tips used were both OMCL-AC200TS (commercially available from Olympus) and Bruker FESPP and TESP silicon cantilevers. **Scanning Emission Microscopy (SEM)** images were obtained with a Philips XL30 S-FEG instrument.

Starting materials. Chemicals were purchased from commercial suppliers and used without further purification. Solid hygroscopic reagents were dried in a vacuum oven before use. Reaction solvents were thoroughly dried before use using standard methods.

Synthesis and characterization

The synthesis and characterization of compounds **1**, **B2**, **C**, and **G** have been previously reported.¹

Synthetic procedure and characterization data of the chains decorating the central blocks (L3)



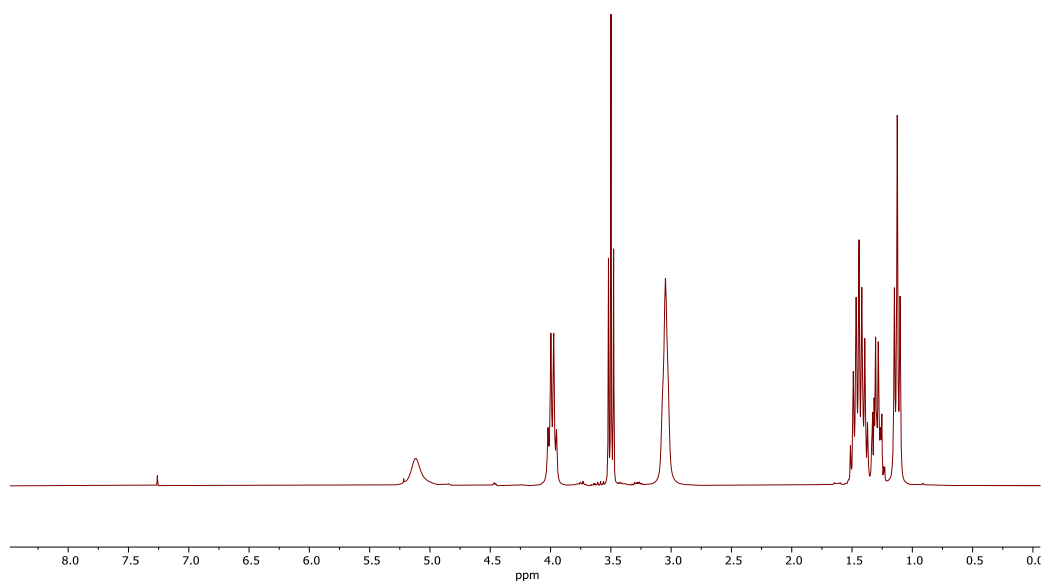
L3.2.² This compound was synthesized by adapting a published procedure.³ Starting from the commercial 5-aminopentanol (3.00 g, 27.63 mmol), it was dissolved with KOH (3.65 g, 55.25 mmol) in 30 mL of water and cooled with an ice bath. Then, ethyl chloroformate (3.09 g, 27.63 mmol) was added slowly to the mixture. After 3 hours, the reaction was quenched with H_2SO_4 (25 %) until pH 7. Methylene chloride was added to the mixture (3 x 40 mL) and the

phases were separated. The organic solvent was then dried with MgSO_4 and dried over vacuum. The desired product was obtained as a colourless liquid (4.33 g, 90 %).

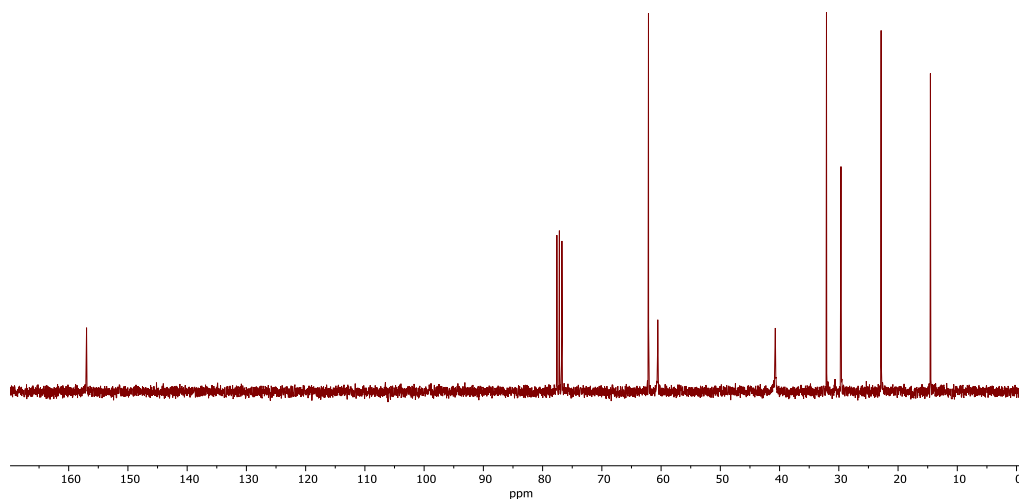
$^1\text{H NMR}$ (300 MHz, CDCl_3) δ (ppm) = 5.02 (s, 1H, $-\text{NH}$), 4.02 (q, $J = 7.1$ Hz, 2H, $\text{CH}_3\text{-CH}_2\text{-OCO}$), 3.55 (t, $J = 6.4$ Hz, 2H, $-\text{CH}_2\text{-OH}$), 3.10 (q, $J = 6.6$ Hz, 2H, $-\text{OCO-NH-CH}_2$), 2.80 (s, 1H, $-\text{OH}$), 1.58 – 1.25 (m, 6H, $-\text{NH-CH}_2\text{-(CH}_2\text{)}_3\text{-CH}_2\text{-OH}$), 1.16 (t, $J = 7.1$ Hz, 3H, $\text{CH}_3\text{-CH}_2\text{-OCO}$).

$^{13}\text{C NMR}$ (76 MHz, CDCl_3) δ (ppm) = 157.0, 62.1, 60.6, 40.7, 32.1, 29.6, 22.8, 14.5.

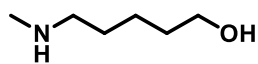
HRMS (EI-TOF): Calculated for $\text{C}_8\text{H}_{17}\text{NO}_3 = 175.1208$, found $m/z = 175.1216$ $[\text{M}]^+$.



$^1\text{H NMR}$ of compound **L3.2** in CDCl_3 (298K, 300MHz).

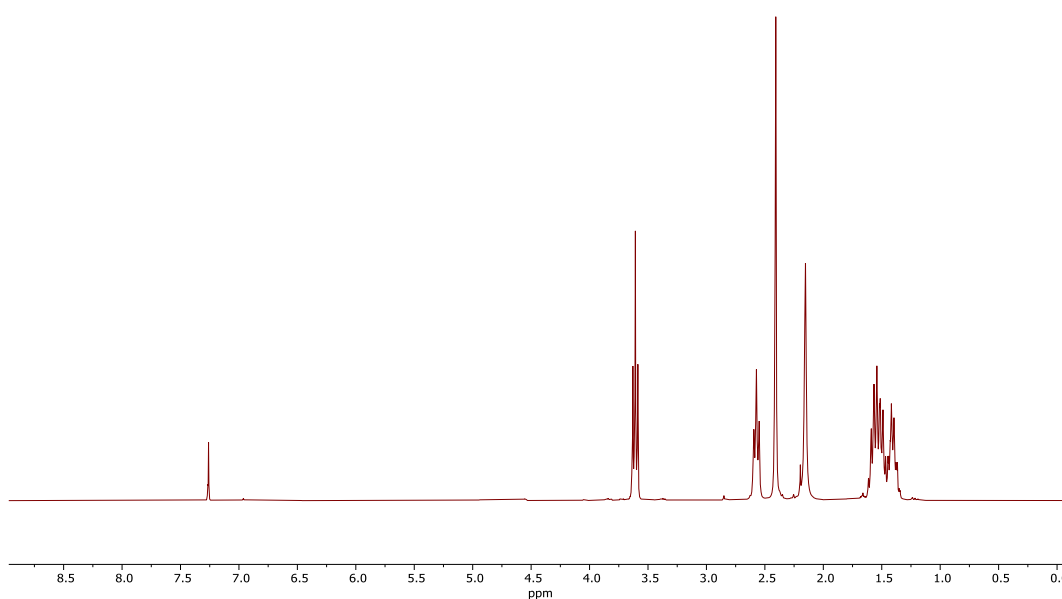


$^{13}\text{C NMR}$ of compound **L3.2** in CDCl_3 (298K, 76MHz).

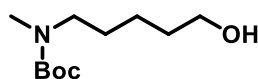


L3.1.³ This compound was synthesized by adapting a published procedure.³ The previous compound **L3.2** (2.15 g, 12.27 mmol) was dissolved in 15 mL of dry THF under Ar atmosphere and cooled with an ice bath. Then LiAlH₄ 1M in THF/hexanes (24.54 mL, 24.54 mmol) was added to the crude reaction dropwise. The reaction was stirred overnight under Ar atmosphere at 65 °C. After this time, the reaction was neutralized with NH₃ (28 %) and KOH 1 M, and the crude was extracted several times with CH₂Cl₂ (3 x 70 mL). The solvent was eliminated under reduced pressure and the crude obtained was purified by distillation, obtaining 1.20 g of a colourless liquid (83 %).

¹H NMR (300 MHz, CDCl₃) δ (ppm) = 5.29 (s, 1H, -OH), 3.60 (t, *J* = 6.4 Hz, 2H, -CH₂-OH), 2.57 (t, *J* = 6.9 Hz, 2H, CH₃-NH-CH₂), 2.40 (s, 3H, CH₃-NH), 2.06 (s, 1H, -NH), 1.65 – 1.30 (m, 6H, CH₃-NH-CH₂-(CH₂)₃-CH₂-OH).



¹H NMR of compound **L3.1** in CDCl₃ (298K, 300MHz).

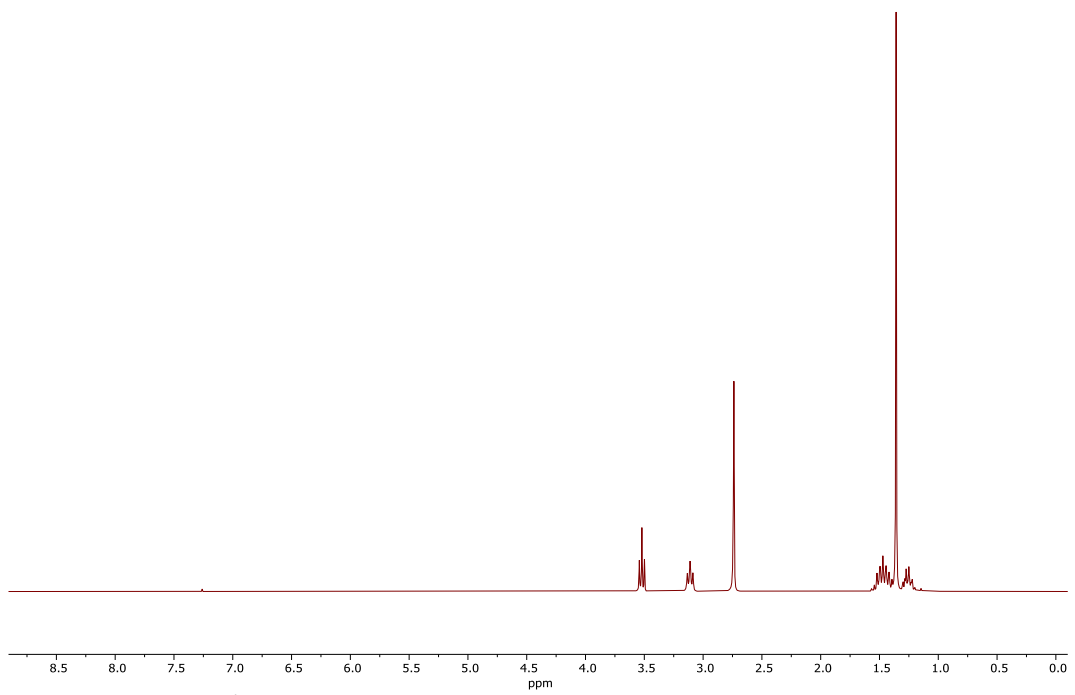


L3. This compound was synthesized by adapting a published procedure.⁴ Protection of the amino group was carried out by dissolving **L3.1** (1.20 g, 10.24 mmol) together with NaOH (1.27 g, 30.72 mmol) and di-*tert*-butyl dicarbonate (2.53 g, 11.26 mmol) in 24 mL of dioxane/water (5:1) mixture. The reaction was allowed to stir overnight at room temperature. Once the reaction was finished, it was quenched with HCl (5 % v/v) until pH 5. Dichloromethane was added and the organic phase was washed with water and brine, dried with MgSO₄ and the solvent was eliminated under reduced pressure. The crude was purified by column chromatography with cyclohexane/AcOEt (1:1) as eluent, obtaining a yellowish liquid (2.10 g, 94 %).

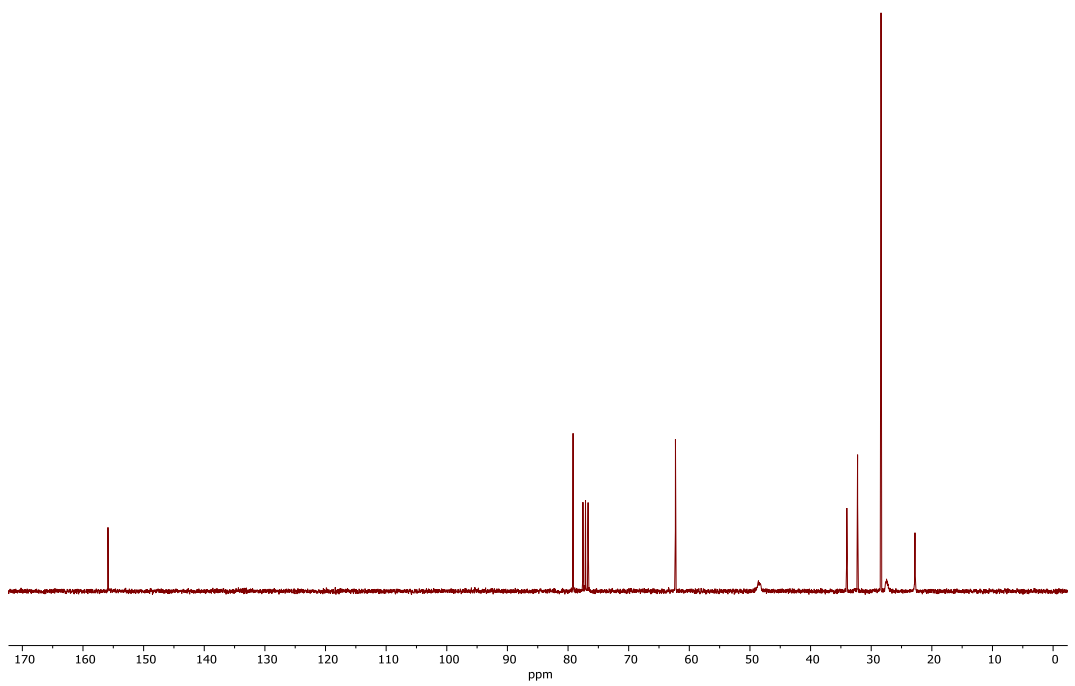
¹H NMR (300 MHz, CDCl₃) δ (ppm) = 3.63 (t, *J* = 6.5 Hz, 2H, -CH₂-OH), 3.20 (t, *J* = 6.0 Hz, 2H, CH₃-NBoc-CH₂), 2.82 (s, 3H, CH₃-N), 1.66 – 1.27 (m, 15H, CH₃-NH-CH₂-(CH₂)₃-CH₂-OH, N-Boc).

¹³C NMR (76 MHz, CDCl₃) δ (ppm) = 155.9, 79.2, 62.3, 48.5, 34.1, 32.3, 28.4, 27.5, 22.8.

HRMS (EI-TOF): Calculated for C₁₁H₂₃NO₃ = 217.1678, found *m/z* = 217.1677 [M]⁺.

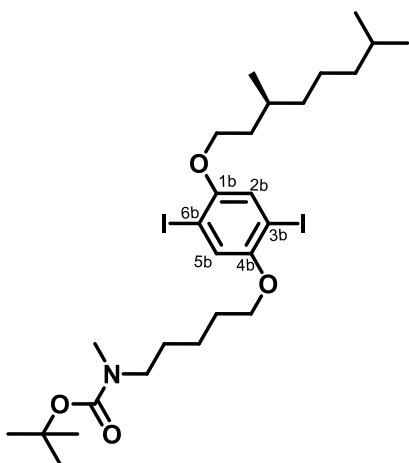


^1H NMR of compound **L3** in CDCl_3 (298K, 300MHz).



^{13}C NMR of compound **L3** in CDCl_3 (298K, 76MHz).

Synthetic procedure and characterization data of the central block (B3)



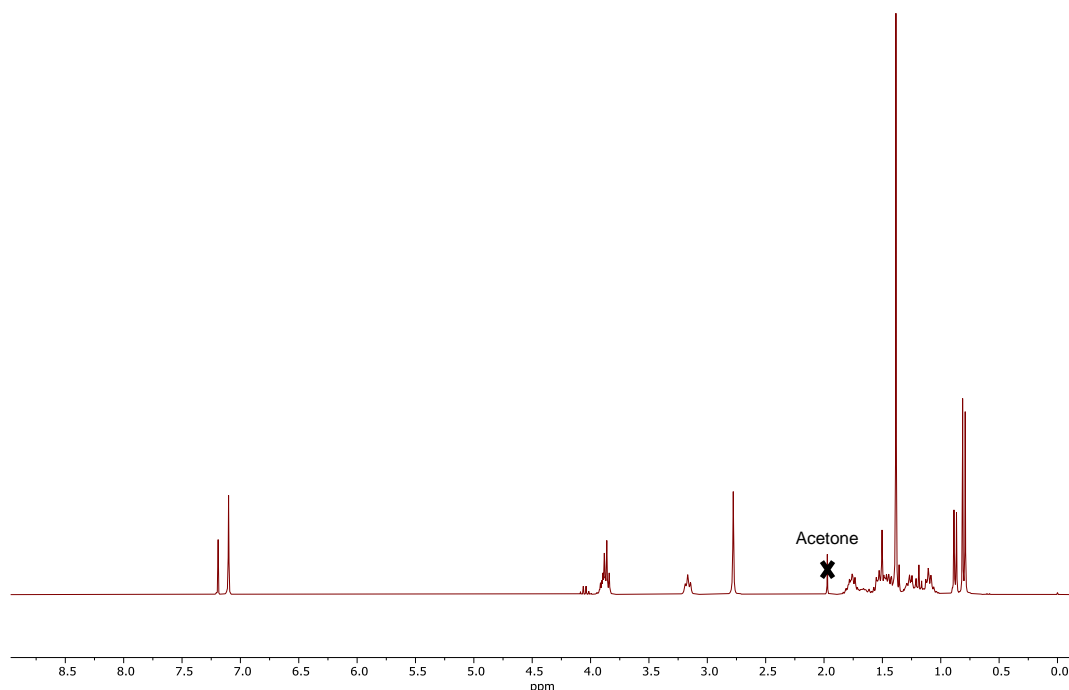
B3. This compound was synthesized by adapting a published procedure.⁵ To a round bottom flask was added **1**¹ (505.0 mg, 1.01 mmol), **L3** (240.38 mg, 1.11 mmol), PPh₃ (290.14 mg, 1.11 mmol) and 2 mL of dry THF. The reaction vessel was then introduced into a 40-kHz sonication bath (Elmasonic TI-H-10) and sonicated for 10 minutes. Then, diisopropylazodicarboxylate (0.23 mL, 1.11 mmol) was added to the solution. The solution was sonicated at room temperature for 15 minutes. Cold cyclohexane was added after this in order to quench the reaction and precipitate the majority of triphenylphosphine oxide byproduct, which was filtrated, and the crude was purified by column chromatography with methylene chloride/cyclohexane (2:1) as eluent, affording **B3** as an orange

solid (430 mg, 61 %).

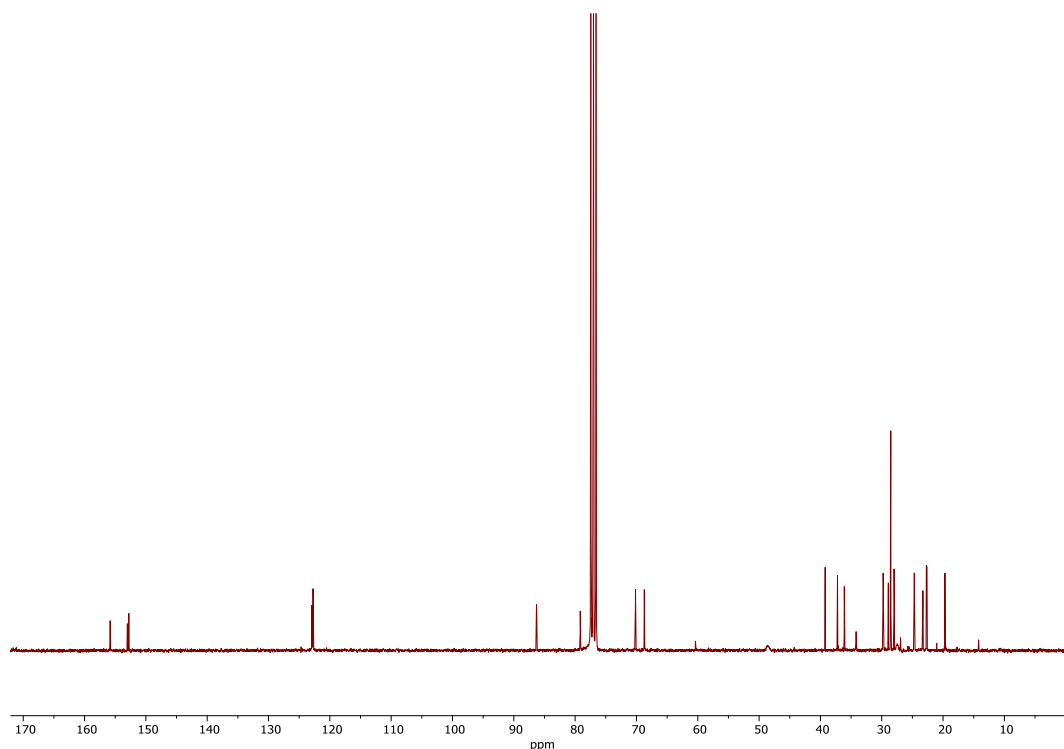
¹H NMR (300 MHz, CDCl₃) δ (ppm) = 7.17 (s, 2H, **H**^{2b, 5b}), 3.95 (m, 4H, C^{1b}-O-CH₂, C^{4b}-O-CH₂), 3.24 (t, *J* = 6.9 Hz, 2H, Boc-N-CH₂), 2.85 (s, 3H, CH₃-N), 1.94 – 1.05 (m, 25H, ^tBu-OCO-N-CH₂-(CH₂)₃, C^{1b}-O-CH₂-CH₂-CH-(CH₂)₃-CH), 0.95 (d, *J* = 6.5 Hz, 3H, *CH-CH₃), 0.87 (d, *J* = 6.6 Hz, 6H, CH-(CH₃)₂).

¹³C NMR (76 MHz, CDCl₃) δ (ppm) = 156.0, 153.2, 152.9, 123.1, 122.9, 86.45, 86.43, 79.3, 70.3, 68.9, 60.5, 39.4, 37.4, 37.2, 36.2, 34.3, 29.9, 29.1, 28.7, 28.1, 27.1, 24.8, 23.4, 22.9, 22.8, 21.2, 19.8, 14.4.

HRMS (APCI+): Calculated for C₂₇H₄₅I₂NO₄ = 702.1516, found *m/z* = 702.1525 [M+H]⁺.

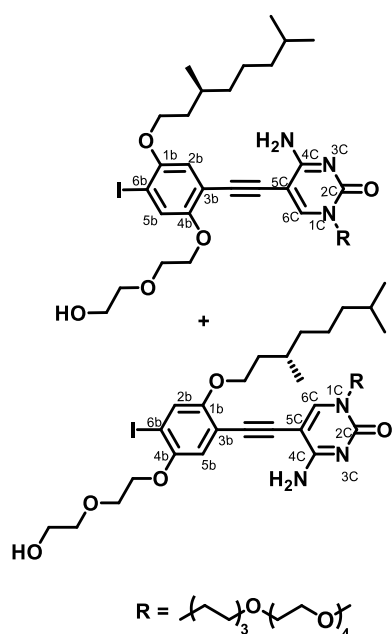


¹H NMR of compound **B3** in CDCl₃ (298K, 300MHz).



^{13}C NMR of compound **B3** in CDCl_3 (298K, 76MHz).

Synthetic procedures and characterization data of building block-cytosine derivatives (BC)



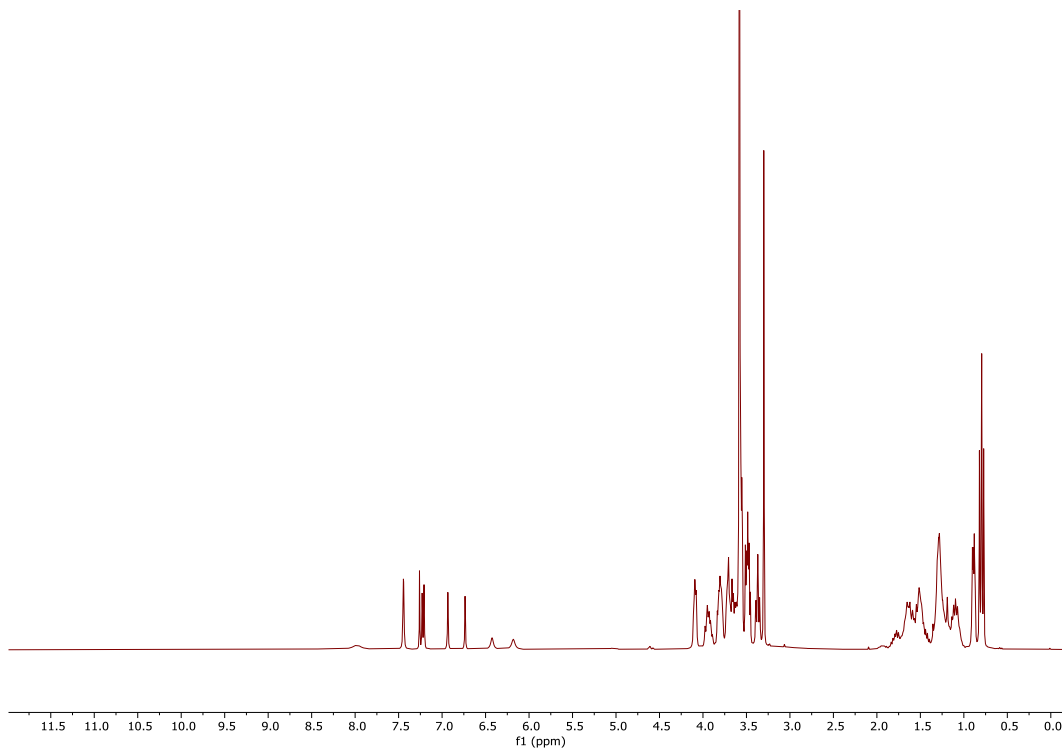
B2C. Central block **B2¹** (871.0 mg, 1.476 mmol), $\text{Pd}(\text{PPh}_3)_2\text{Cl}_2$ (5.2 mg, 0.005 mmol) and CuI (0.7 mg, 0.005 mmol) were dissolved in a 4:1 mixture of THF/NEt_3 (4:1, 20 mL) previously deoxygenated by 3 freeze-pump-thaw cycles with argon. Then, a solution of compound **C¹** (157.0 mg, 0.369 mmol) was added dropwise to the previous mixture, and it was stirred under argon at room temperature until completion. Then, reaction was filtrated over celite and the corresponding solvent was eliminated under vacuum. The resulting residue was purified by column chromatography using $\text{CHCl}_3/\text{MeOH}$ (4:1) as eluent with an additionally 0.1 % of acetic acid in a final step, affording compound **B2C** as a yellowish solid (166 mg, 51 %)

^1H NMR (300 MHz, CDCl_3) δ (ppm)= 7.98 (s, 1H, OH), 7.45, 7.43 (2xs, 1H, $\text{H}^{6\text{C}}$), 7.23, 7.21 (2xs, 1H, $\text{H}^{5\text{b}}$), 6.84, 6.82 (2xs, 1H, $\text{H}^{2\text{b}}$), 6.43 (s, 1H, $\text{C}^4\text{CNH-H}$), 6.18 (s, 1H, $\text{C}^4\text{CNH-H}$), 4.09 (m, 2H, $\text{O}^{4\text{b}}\text{-CH}_2$), 4.01 – 3.87 (m, 2H, $\text{O}^{1\text{b}}\text{-CH}_2$), 3.80 (m, 4H, $\text{O}^{4\text{b}}\text{CH}_2\text{-CH}_2$, $\text{CH}_2\text{-OH}$), 3.75 – 3.52 (m, 16H, $\text{-CH}_2\text{-CH}_2\text{OH}$, $\text{-(OCH}_2\text{CH}_2)_3\text{OCH}_2\text{-CH}_2\text{OCH}_3$), 3.49 (m, 4H, $\text{N}^{1\text{C}}\text{-CH}_2$, $\text{CH}_2\text{-OCH}_3$), 3.37 (m, 2H, $\text{N}^{1\text{C}}\text{C}_5\text{H}_{10}\text{-CH}_2$), 3.30 (s, 3H, O-CH_3), 1.87 – 1.39 (m, 10H, $\text{O}^{1\text{b}}\text{CH}_2\text{-CH}_2\text{CH-}$, $\text{-CH-(CH}_3)_2$, $\text{N}^{1\text{C}}\text{CH}_2\text{-CH}_2$, $\text{N}^{1\text{C}}\text{C}_3\text{H}_6\text{-(CH}_2)_2$), 1.38 – 0.99 (m, 8H, $\text{-(CH}_2)_3\text{-CH(CH}_3)_2$, $\text{N}^{1\text{C}}\text{C}_2\text{H}_4\text{-CH}_2$), 0.91, 0.88 (2xd, $J = 6.4$ Hz, 3H, *CH-CH_3), 0.81, 0.78 (2xd, $J = 6.6$ Hz, 6H, $\text{CH-(CH}_3)_2$).

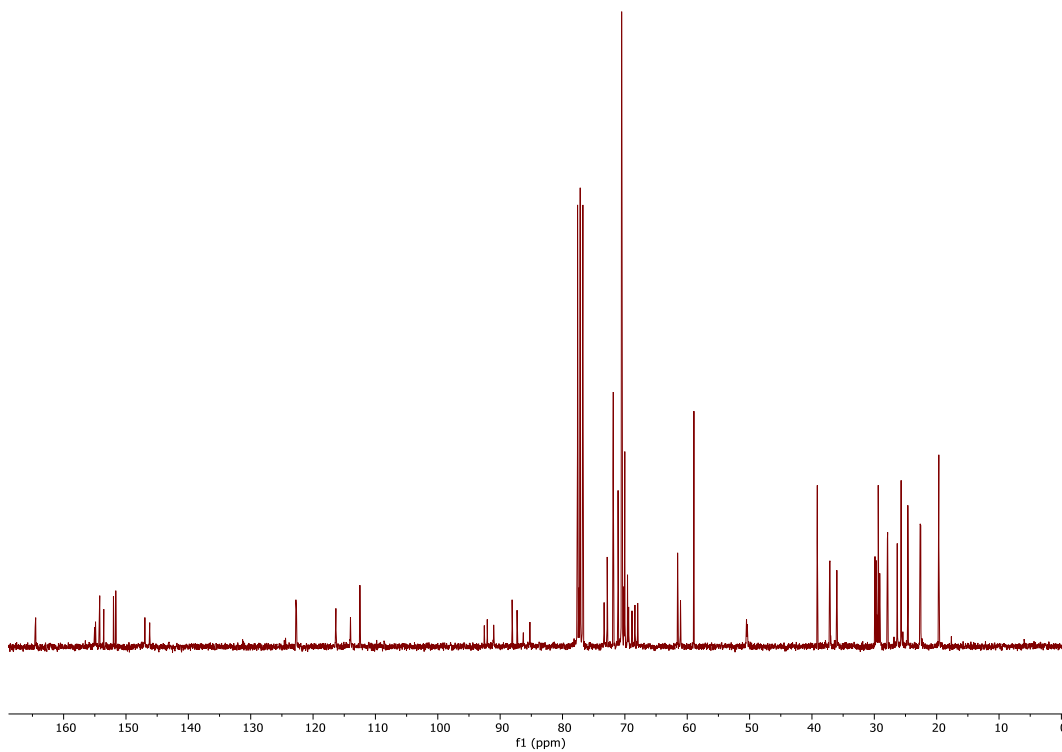
^{13}C NMR (76 MHz, CDCl_3) δ (ppm) = 163.4, 163.3, 153.9, 153.7, 153.1, 152.4, 150.8, 150.5, 145.8, 145.0, 121.6, 121.5, 115.2, 112.8, 111.3, 91.4, 90.9, 89.9, 86.9, 86.1, 85.1, 84.1, 76.2, 72.2, 71.7, 70.7, 69.9, 69.4, 69.3, 69.2,

69.0, 68.8, 68.4, 68.2, 67.7, 67.2, 66.8, 60.4, 59.9, 57.8, 49.3, 49.2, 38.0, 36.0, 35.95, 34.88, 34.85, 28.7, 28.6, 28.4, 28.2, 28.0, 26.8, 26.70, 25.2, 24.5, 24.3, 23.5, 21.53, 21.50, 21.43, 21.39, 18.5.

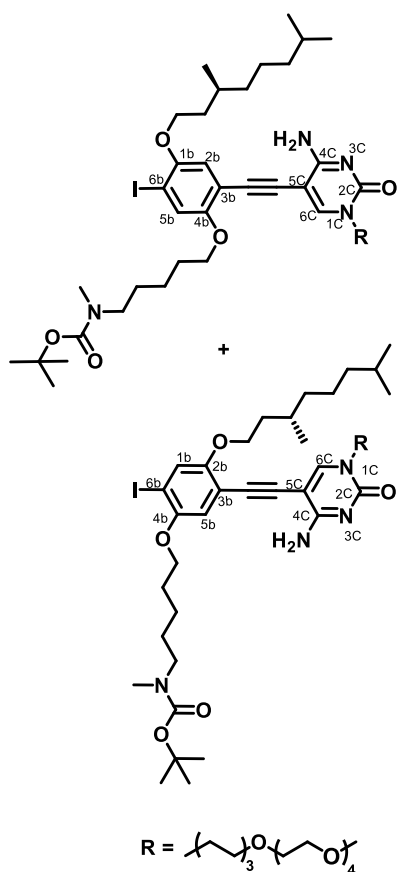
HRMS (MALDI-TOF), (DCTB + NaI): Calculated for $C_{41}H_{66}IN_3O_{10}Na$ = 910.3793, found m/z = 910.3665 $[M+Na]^+$.



1H NMR of compound **B2C** in $CDCl_3$ (298K, 300MHz).



^{13}C NMR of compound **B2C** in $CDCl_3$ (298K, 76MHz).

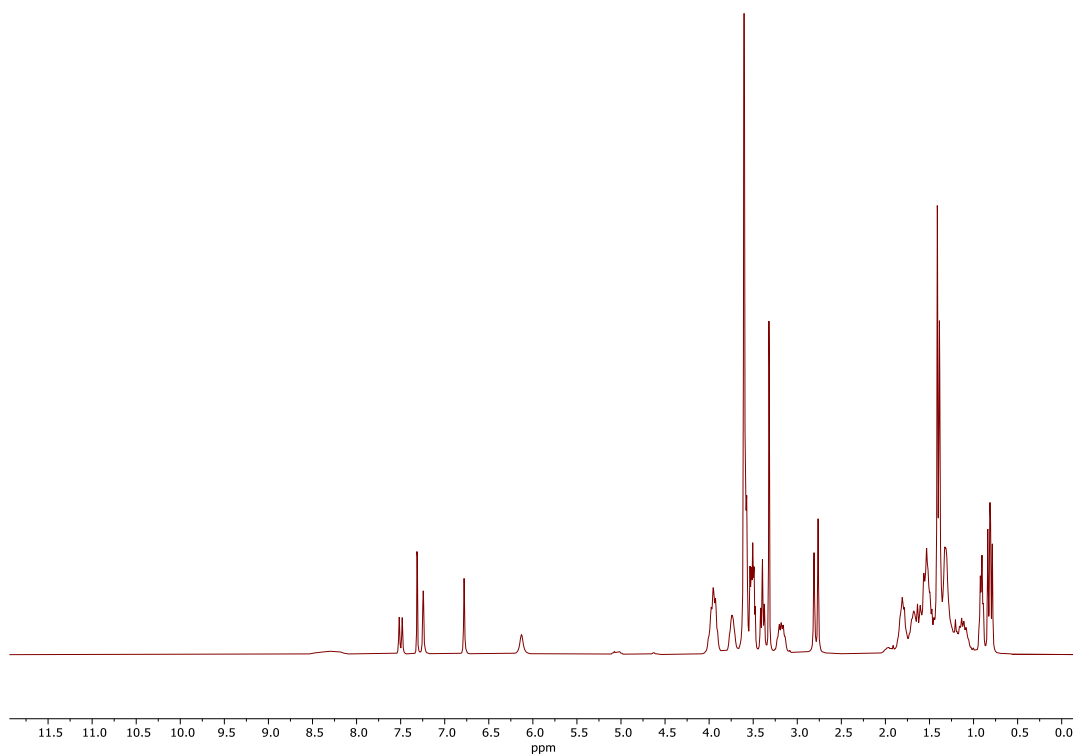


B3C. 20 mL of a dry THF/ NEt_3 (4:1) mixture, previously deoxygenated, was added to a round-bottom flask containing **B3** (741.81 mg, 1.06 mmol), $\text{Pd}(\text{PPh}_3)_2\text{Cl}_2$ (4.95 mg, 0.007 mmol) and CuI (0.4 mg, 0.004 mmol). The mixture was stirred at room temperature under argon for a few minutes. Then, **C1** (150.0 mg, 0.35 mmol) was added, previously dissolved in 5 mL of THF/ NEt_3 mixture. The reaction was stirred overnight at 40°C . Once its completion, the crude was filtrated over celite and the solvent was evaporated under reduced pression. The resulting solid was purified by column chromatography with $\text{CHCl}_3/\text{MeOH}$ (20:1) as eluent, giving rise to an orange oil (230.0 mg, 65 %).

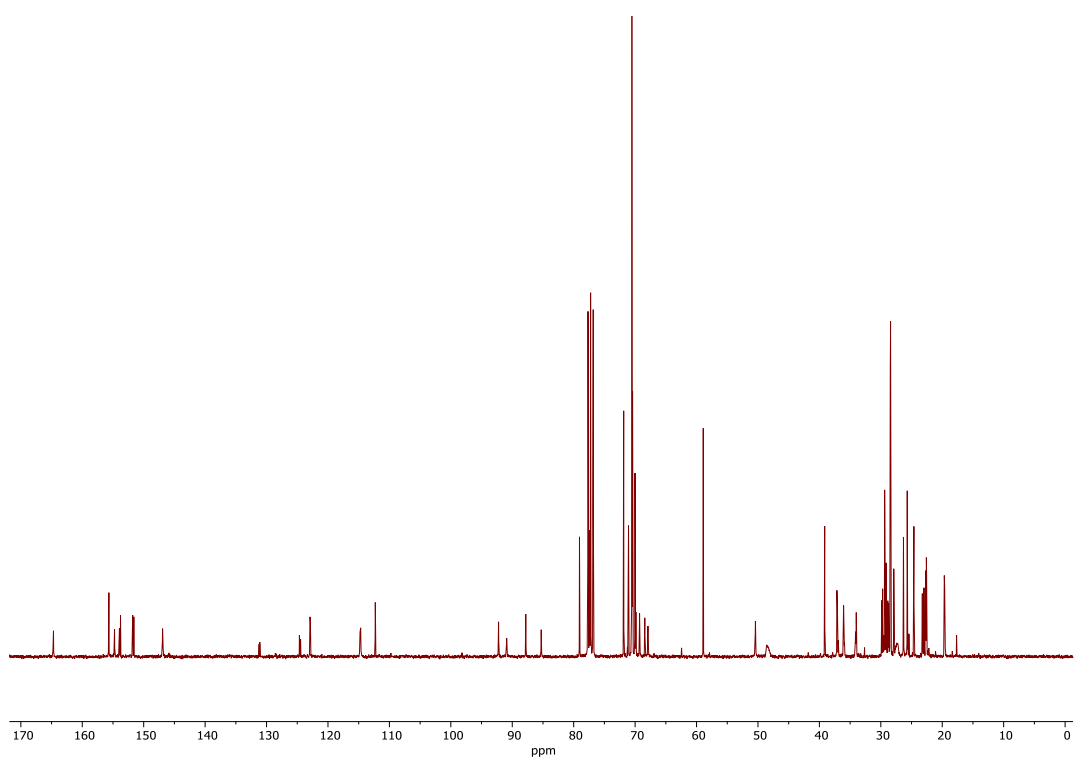
^1H NMR (300 MHz, CDCl_3) δ (ppm)= 8.33 (bs, 1H, $\text{C}^4\text{C}^{\text{N}}\text{H}-\text{H}$), 7.53, 7.50 (2xs, 1H $\text{H}^{6\text{C}}$), 7.33, 7.32 (2xs, 1H, $\text{H}^{5\text{b}}$), 6.79 (s, 1H, $\text{H}^{2\text{b}}$), 6.14 (s, 1H, $\text{C}^4\text{C}^{\text{N}}\text{H}-\text{H}$), 3.97 (q, $J = 7.16$ Hz, 4H, $\text{O}^{4\text{b}}-\text{CH}_2$, $\text{O}^{1\text{b}}-\text{CH}_2$), 3.69 – 3.46 (m, 18H, $\text{N}^{1\text{C}}-\text{CH}_2$, $-(\text{OCH}_2\text{CH}_2)_4\text{OCH}_3$), 3.41 (t, 2H, $J = 6.49$ Hz, $\text{N}^{1\text{C}}\text{C}_5\text{H}_{10}-\text{CH}_2$), 3.34, 3.33 (2xs, 3H, $-(\text{OCH}_2\text{CH}_2)_4\text{OCH}_3$), 3.20 (dt, 2H, $J = 12.9$ Hz, $J = 6.75$ Hz, $\text{O}^{4\text{b}}-(\text{CH}_2)_4-\text{CH}_2$), 2.83, 2.78 (2xs, 3H, $\text{O}^{4\text{b}}-(\text{CH}_2)_5-\text{N}-\text{CH}_3$), 1.90 – 1.46 (m, 10H, $\text{O}^{1\text{b}}\text{CH}_2-\text{CH}_2\text{CH}-$, $-\text{CH}(\text{CH}_3)_2$, $\text{N}^{1\text{C}}\text{CH}_2-\text{CH}_2$, $\text{N}^{1\text{C}}\text{C}_3\text{H}_6-(\text{CH}_2)_2$), 1.43, 1.40 (2xs, 9H, **N-Boc**), 1.37 – 1.06 (m, 15H, $-(\text{CH}_2)_3-\text{CH}(\text{CH}_3)_2$, $\text{N}^{1\text{C}}\text{C}_2\text{H}_4-\text{CH}_2$, $t\text{Bu}-\text{OCO}-\text{N}-\text{CH}_2-(\text{CH}_2)_3$), 0.92 (m, 3H, $^*\text{CH}-\text{CH}_3$), 0.84, 0.81 (2xd, $J = 6.6$ Hz, 6H, $\text{CH}-(\text{CH}_3)_2$).

^{13}C NMR (76 MHz, CDCl_3) δ (ppm) = 164.7, 164.68, 155.7, 155.67, 154.8, 154.0, 153.8, 151.8, 151.6, 146.9, 131.2, 131.1, 124.6, 124.5, 122.9, 122.86, 114.8, 114.7, 112.3, 92.2, 90.9, 87.8, 87.78, 85.3, 79.1, 79.0, 77.4, 71.9, 71.2, 71.1, 70.5, 70.49, 70.4, 70.02, 69.9, 69.3, 68.4, 67.9, 62.4, 58.9, 50.4, 39.1, 37.2, 37.1, 37.0, 36.9, 36.1, 36.0, 34.1, 34.0, 32.6, 29.8, 29.7, 29.6, 29.5, 29.5, 29.4, 29.1, 28.9, 28.7, 28.5, 28.4, 27.9, 27.8, 26.3, 25.9, 25.7, 25.6, 25.57, 25.43, 25.40, 24.6, 23.2, 23.0, 22.7, 22.6, 22.6, 22.6, 22.2, 21.1, 19.7, 19.6, 19.5, 18.4, 17.7, 17.6.

HRMS (APCI+): Calculated for $\text{C}_{48}\text{H}_{79}\text{N}_4\text{O}_{10}$ = 999.4919, found m/z = 999.4920 $[\text{M}+\text{H}]^+$.

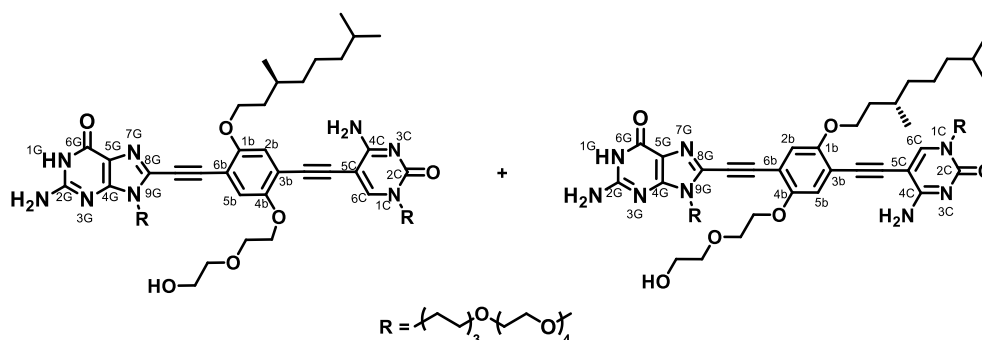


^1H NMR of compound **B3C** in CDCl_3 (298K, 300MHz).



^{13}C NMR of compound **B3C** in CDCl_3 (298K, 76MHz).

Synthetic procedures and characterization data of G-C final compounds

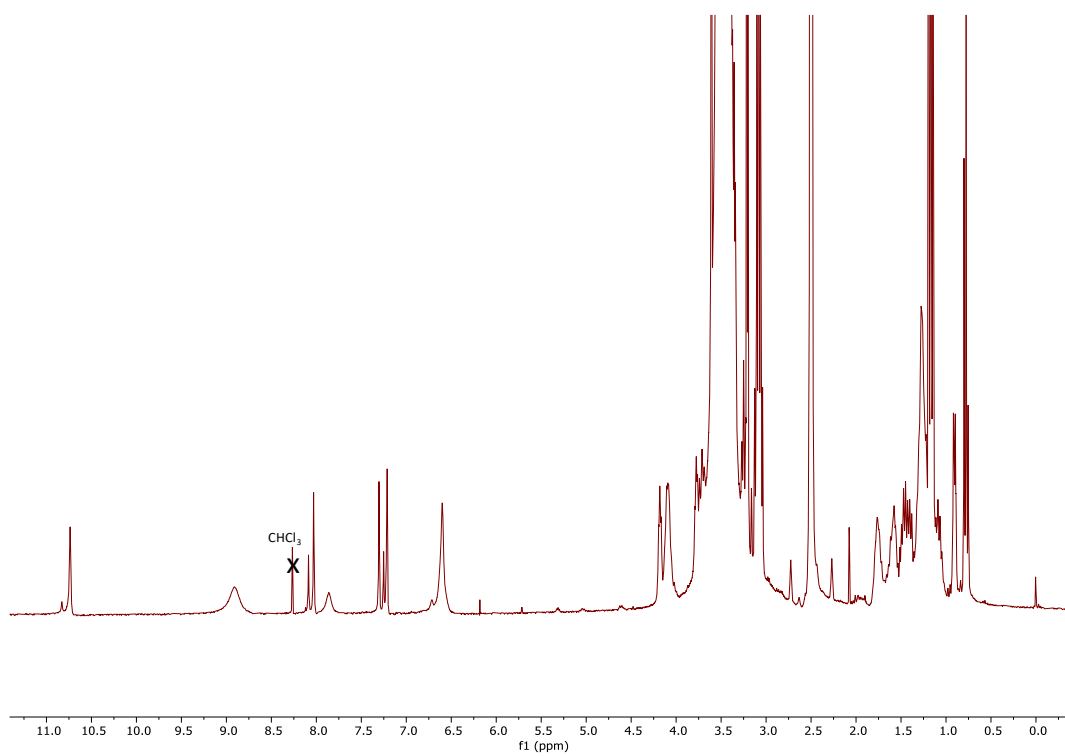


GC2. B2C (130.51 mg, 0.147 mmol), Pd(PPh₃)₂Cl₂ (2.00 mg, 0.003 mmol) y Cul (0.4 mg, 0.001 mmol) were dissolved in 3 mL of THF/NEt₃ (4:1) mixture previously deoxygenated by 3 cycles *freeze-pump-thaw*. Then, **G** (137.00 mg, 0.294 mmol), dissolved in 5 mL of THF/NEt₃, was added dropwise to the reaction mixture, which stirred at room temperature until **G** was consumed. Then, the mixture was filtrated over celite and the solvent was removed under reduced pression. The product was purified by column chromatography with a gradient of CHCl₃/MeOH. The final product was washed with Et₂O (210 mg, 55 %).

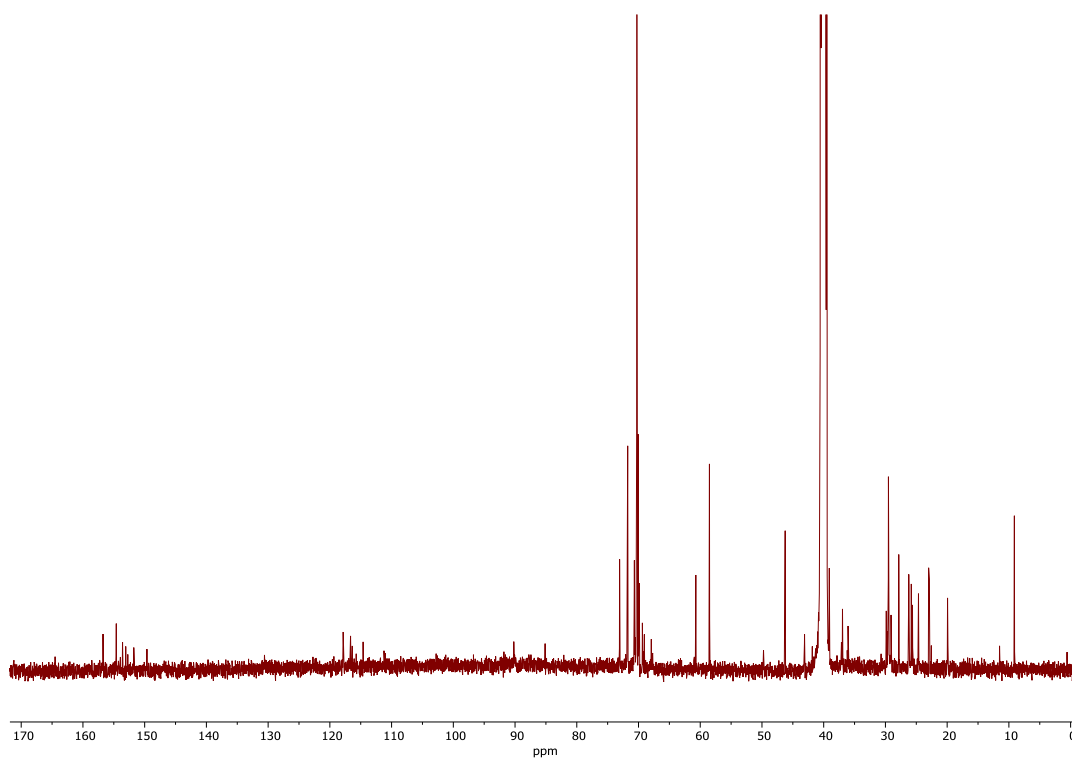
¹H NMR (300 MHz, DMSO-*d*₆) δ (ppm) = 10.73 (s, 1H, NH^{1G}), 8.90 (s, 1H, C^{4C}NH-**H**), 8.08, 8.02 (2xs, 1H, **H**^{6C}), 7.85 (s, 1H, C^{4C}NH-**H**), 7.31 (s, 1H, **H**^{6b}), 7.24, 7.20 (2xs, 1H, **H**^{2b}), 6.59 (br, 3H, -OH, C^{2G}-NH₂), 4.18 (m, 2H, O^{4b}-CH₂), 4.09 (br, 4H, N^{9G}-CH₂, O^{1b}-CH₂), 3.77 (m, 4H, O^{4b}CH₂-CH₂, CH₂-OH), 3.65-3.30 (br, 46H, CH₂CH₂-OH CH₂-OCH₃, N^{1C}-CH₂, -CH₂(OCH₂CH₂)₃-CH₂CH₂-OCH₃, O-CH₃), 1.81 - 1.37 (m, 16H, O^{1b}CH₂-CH₂CH-, -CH-(CH₃)₂, N^{1C}, ^{9G}CH₂-CH₂, N^{1C}, ^{9G}C₃H₆-(CH₂)₂) 1.25 (m, 10H, -(CH₂)₃-CH(CH₃)₂, N^{1C}, ^{9G}C₂H₄-CH₂), 0.92 (d, *J* = 6.2 Hz, 3H, *CH-CH₃), 0.79 (d, *J* = 6.4 Hz, 6H, CH-(CH₃)₂).

¹³C NMR (126 MHz, DMSO-*d*₆) δ (ppm) = 156.2, 154.1, 153.1, 152.6, 152.2, 151.3, 149.1, 130.1, 117.4, 116.1, 115.8, 115.2, 114.1, 110.7, 91.3, 89.7, 84.6, 72.6, 71.5, 71.2, 70.2, 70.1, 69.79, 69.77, 69.74, 69.69, 69.6, 69.45, 69.38, 68.9, 68.6, 67.4, 60.2, 58.01, 57.99, 49.2, 45.7, 42.6, 41.4, 38.6, 36.6, 36.5, 35.7, 35.6, 29.4, 29.24, 29.21, 29.01, 28.97, 28.6, 28.5, 27.3, 25.7, 25.3, 25.14, 25.11, 24.14, 24.11, 22.5, 22.45, 22.38, 22.34, 22.09, 22.06, 22.02, 19.44, 19.38, 11.0, 8.6.

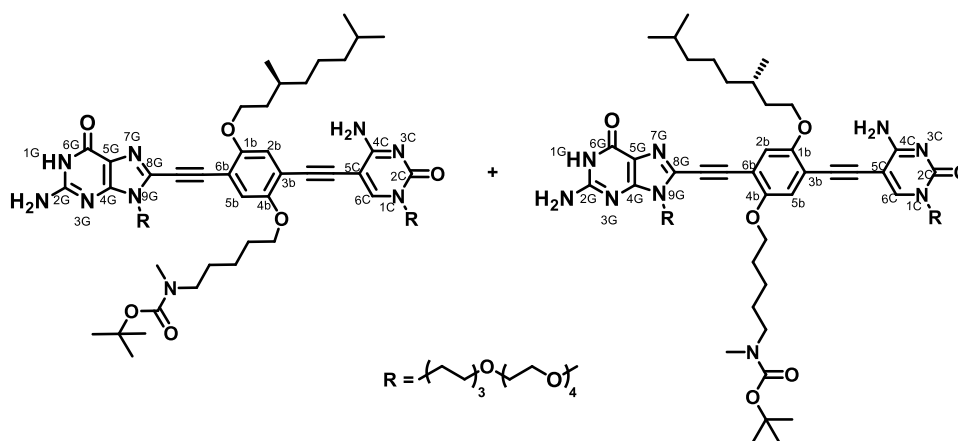
HRMS (MALDI-TOF), (DCTB + NaI): Calculated for C₆₃H₁₀₀N₈O₁₆Na = 1247.7257, found *m/z* = 1247.7137 [M+Na]⁺.



^1H NMR of compound **GC2** in $\text{DMSO-}d_6$ (298K, 300MHz).



^{13}C NMR of compound **GC2** in $\text{DMSO-}d_6$ (298K, 76MHz).

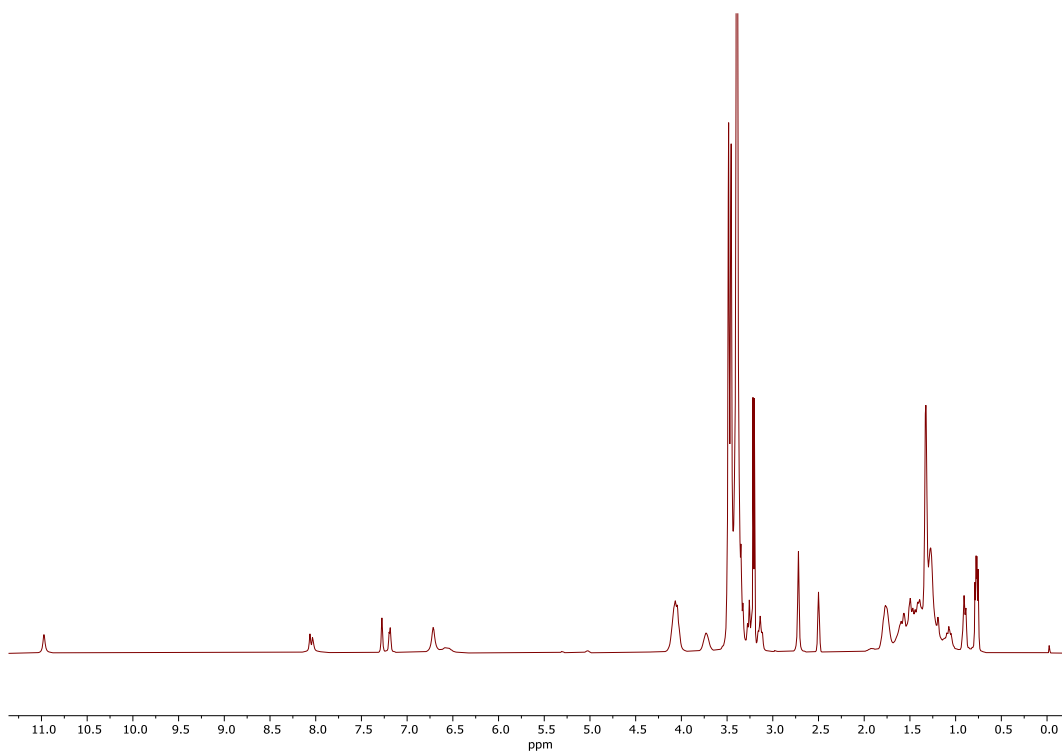


GC3.1. B2C (230.00 mg, 0.230 mmol), Pd(PPh₃)₂Cl₂ (3.00 mg, 0.005 mmol) y Cul (0.43 mg, 0.002 mmol) were dissolved in 10 mL of THF/NEt₃ (4:1) mixture previously deoxygenated by 3 cycles *freeze-pump-thaw*. Then, **G** (117.90 mg, 0.253 mmol), dissolved in 5 mL of THF/NEt₃, was added dropwise to the reaction mixture, which stirred at 40°C until **G** was consumed. Then, the mixture was filtrated over celite and the solvent was removed under reduced pression. The product was purified by column chromatography with CHCl₃/MeOH (10:1) as eluent, obtaining the final product as a yellow solid (190.00 mg, 61 %).

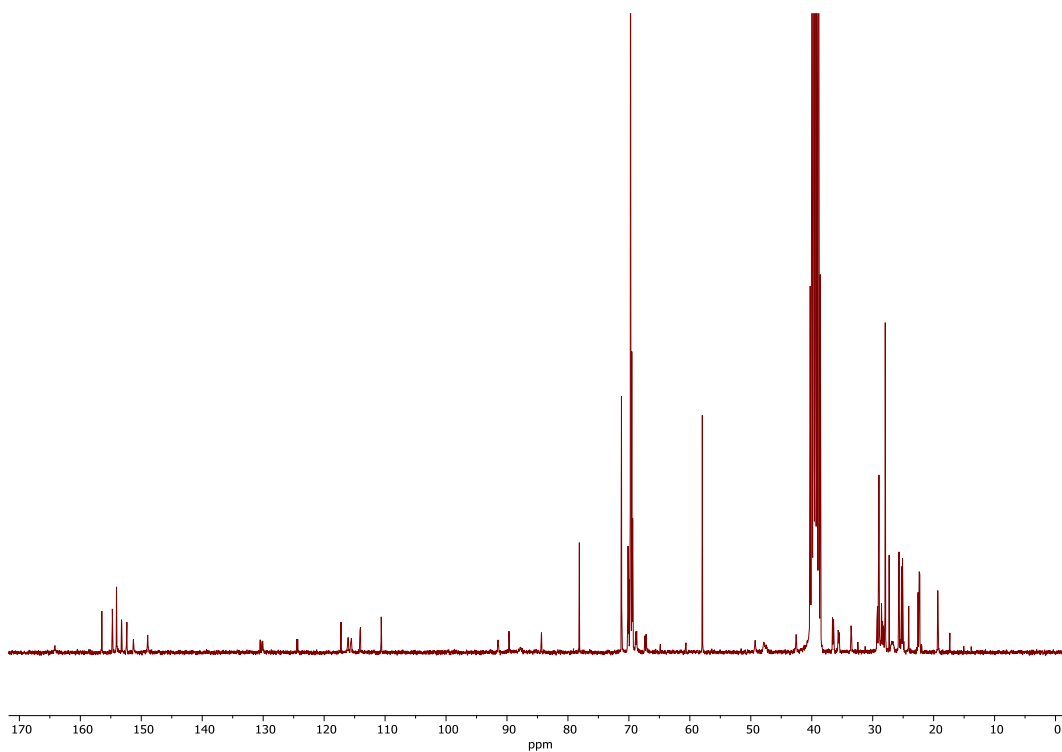
¹H NMR (300 MHz, DMSO-*d*₆) δ (ppm) = 10.97 (s, 1H, NH^{1G}), 8.05 (2xs, 1H, H^{6C}), 7.28 (s, 1H, H^{5b}), 7.20 (2xs, 1H, H^{5b}), 6.71 (s, 2H, C^{2G}-NH₂), 6.57 (s, 1H, C^{4C}NH-H), 4.08 (m, 6H, N^{9G}-CH₂, O^{1b,2b}-CH₂), 3.73 (m, 2H, N^{1C}-CH₂), 3.55 – 3.33 (m, 36H, -(OCH₂CH₂)₄OCH₃, N^{1C,9G}C₅H₁₀-CH₂), 3.30 – 3.07 (m, 8H, -(OCH₂CH₂)₄OCH₃, Boc-N-CH₂), 2.72 (s, 3H, Boc-N-CH₃), 1.88 – 0.98 (m, 35H, O^{1b}CH₂-CH₂CH-, -CH-(CH₃)₂, -(CH₂)₃-CH(CH₃)₂, N^{1C,9G}CH₂-CH₂, N^{1C,9G}C₃H₆-(CH₂)₂, N^{1C,9G}C₂H₄-CH₂, ^tBu-OCO-N-CH₂-(CH₂)₃), 0.98 – 0.85 (m, 3H, *CH-CH₃), 0.77 (m, 6H, CH-(CH₃)₂).

¹³C NMR (76 MHz, CDCl₃) δ (ppm) = 156.5, 154.8, 154.7, 154.1, 153.25, 153.21, 152.42, 152.36, 151.3, 149.0, 130.5, 130.4, 130.1, 124.5, 124.3, 117.2, 116.1, 115.5, 114.1, 114.0, 110.6, 91.5, 89.7, 89.6, 84.4, 78.1, 71.2, 70.14, 70.04, 69.74, 69.71, 69.67, 69.5, 69.42, 69.38, 68.9, 68.7, 67.4, 67.2, 64.8, 60.6, 57.9, 49.3, 47.8, 42.6, 36.6, 36.4, 35.6, 35.5, 33.5, 32.4, 29.3, 29.2, 29.0, 28.9, 28.6, 28.4, 28.2, 28.0, 27.3, 26.9, 26.6, 25.72, 25.68, 25.5, 25.3, 25.1, 25.0, 24.9, 24.1, 24.1, 22.6, 22.41, 22.37, 22.30, 22.27, 19.4, 19.32, 19.27, 19.2, 17.3, 15.1, 13.8.

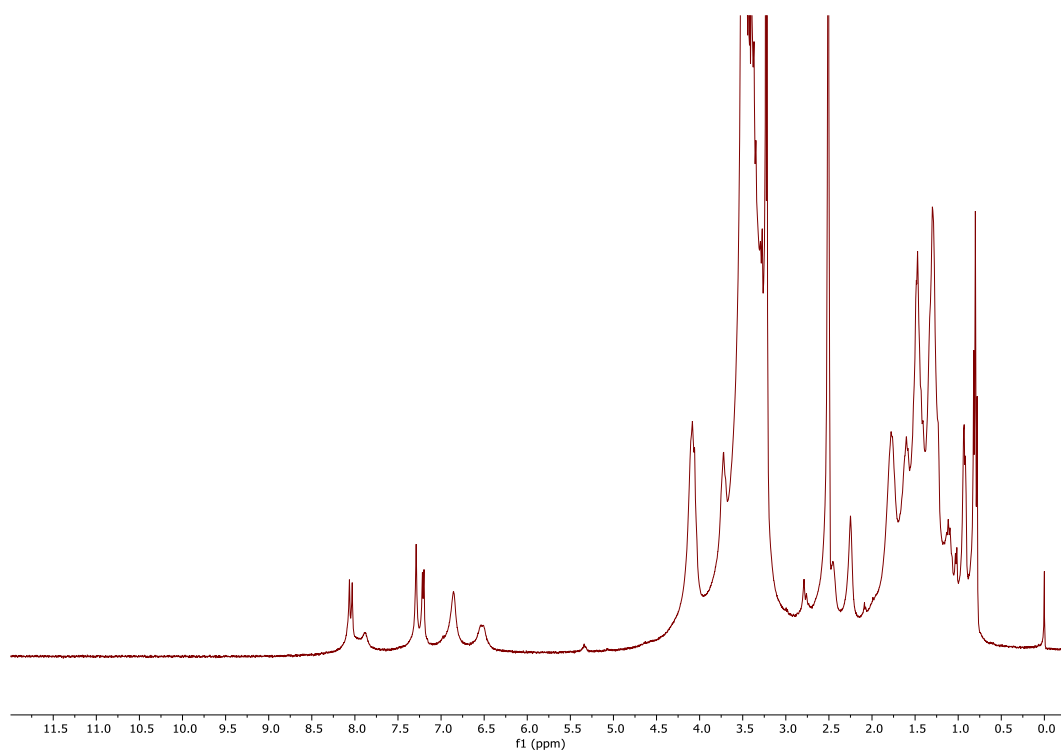
HRMS (APCI+): Calculated for C₇₀H₁₁₃N₉O₁₆ = 1336.838405, found *m/z* = 1336.8355 [M+H]⁺.



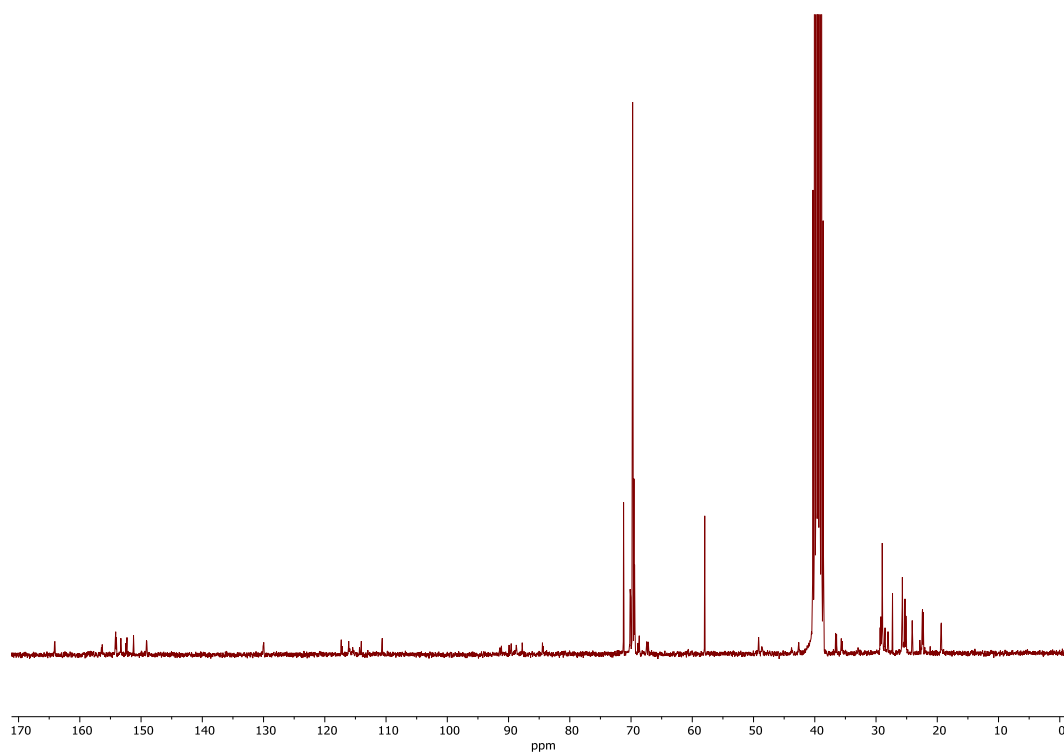
^1H NMR of compound **GC3.1** in $\text{DMSO-}d_6$ (298K, 300MHz).



^{13}C NMR of compound **GC3.1** in $\text{DMSO-}d_6$ (298K, 76MHz).



^1H NMR of compound **GC3** in $\text{DMSO-}d_6$ (298K, 300MHz).



^{13}C NMR of compound **GC3** in $\text{DMSO-}d_6$ (298K, 300MHz).

S1. Preliminary Comparative Studies of the Aggregated States in Water

S1.1. AFM and TEM Microscopy Studies

The morphology and size of the nanostructures formed in aqueous or water/THF solution by the supramolecular polymerization of all the **GC1-GC3** compounds were studied by atomic force and electron transmission microscopy, AFM and TEM, respectively. Samples were dropcasted from diluted solutions onto HOPG (for AFM; mica substrates were also essayed in some cases with similar results) or onto C-formvar Cu grids (for TEM). For room temperature AFM samples, the solution was left stand for 4h and then dried under vacuum at 60°C overnight. For high temperature AFM samples, the corresponding water or water/THF solution at 90°C or 60°C, respectively, was dropcasted onto the substrate previously heated and was keep under vacuum at high temperature overnight. For room temperature TEM samples, the solution was deposited and let incubated for 5 minutes and then most of the solvent was removed with a piece of filter paper. For high temperature TEM samples, the solution at 90°C or 60°C was deposited and the solvent was removed with a piece of filter paper just after dropcasting. In both microscopies, the presence of fibrillary structures was confirmed for room temperature samples, as shown below for each compound in Figures S1A-S1B (**GC1**), Figures S1C-S1D (**GC2**), and Figures S1E-S1F (**GC3**). It was quite frequent to observe heavily bundled fibers, both in AFM and TEM. The last technique revealed a high contrast (darker) profile at the walls of these fibers and a low contrast (lighter) section in the middle, which is fully consistent with tubular architectures. Width dimensions obtained by TEM (5-6 nm; see Figures S1B, S1D and S1F) match rather well the hard, aromatic section expected in our models.¹ However, AFM profiles showed smaller height values than the ones calculated for our system. These smaller values could be the result of the compression of side-chains by the force applied by the AFM probe, effect that has been reported by other research groups,⁶ and the affinity of the assemblies for the surface.

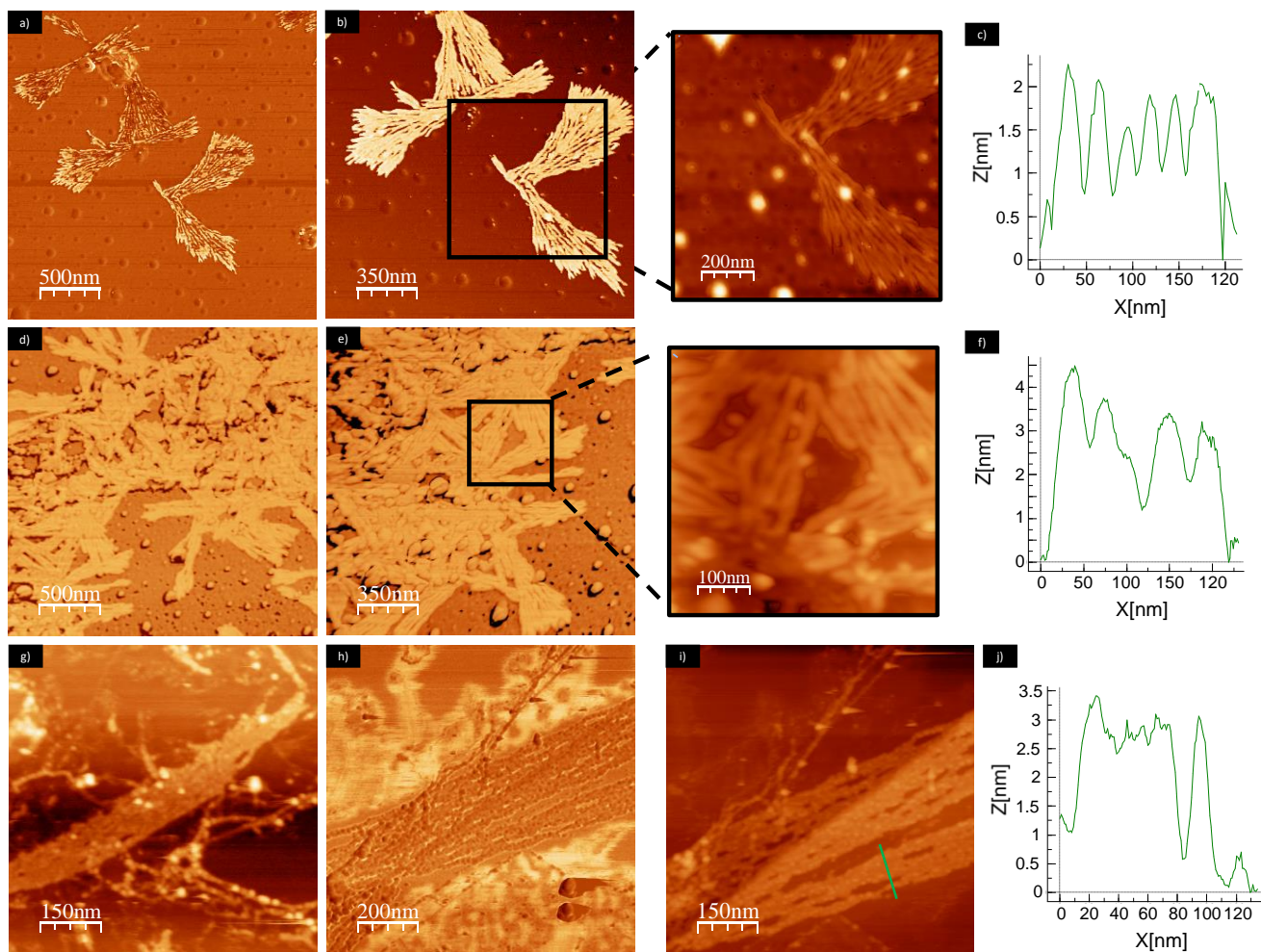


Figure S1A. Phase (a, b, d, e, and h) and height (g, i and zoom in b and e) AFM images of the nanotubes formed by the self-assembly of compound **GC1** ($1.0 \cdot 10^{-5}$ M, H_2O) on HOPG. (c), (f) and (j) Height profile of the aggregates along the grey and green lines in (b), (e) and (i), respectively.

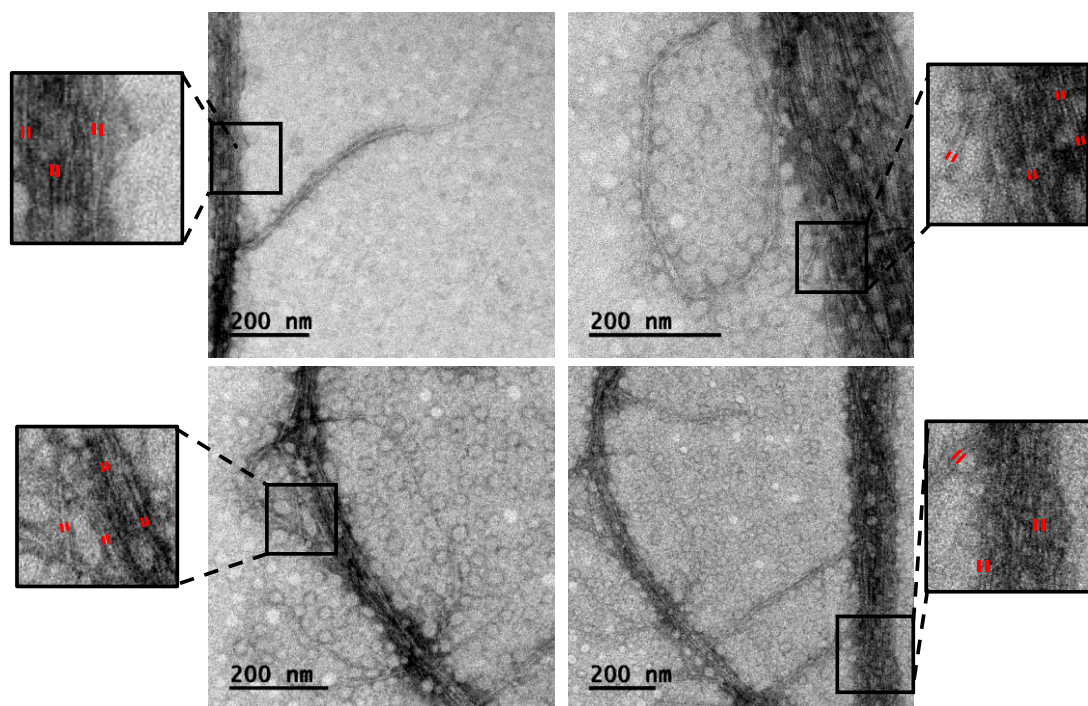


Figure S1B. TEM images of the nanotubes formed by the self-assembly of compound **GC1** ($1.0 \cdot 10^{-6}$ M, H_2O) on C-formvar Cu grids, stained with phosphotungstic acid. Measured nanotube width: ~ 5 nm.

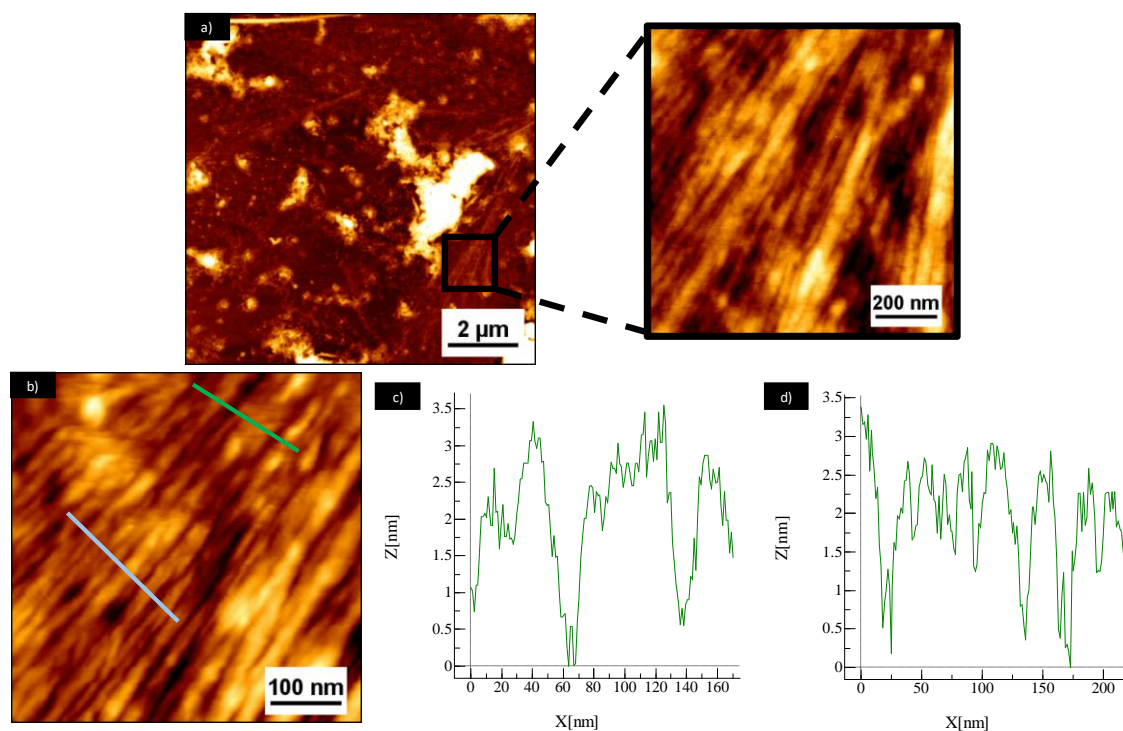


Figure S1C. Height (a, b, and zoom in a) AFM images of the nanotubes formed by the self-assembly of compound **GC2** ($1.0 \cdot 10^{-5}$ M, $\text{H}_2\text{O}/\text{THF}$ 7:3) on HOPG. (c) and (d) Height profile of the aggregates along the green and the blue line, respectively, in (b).

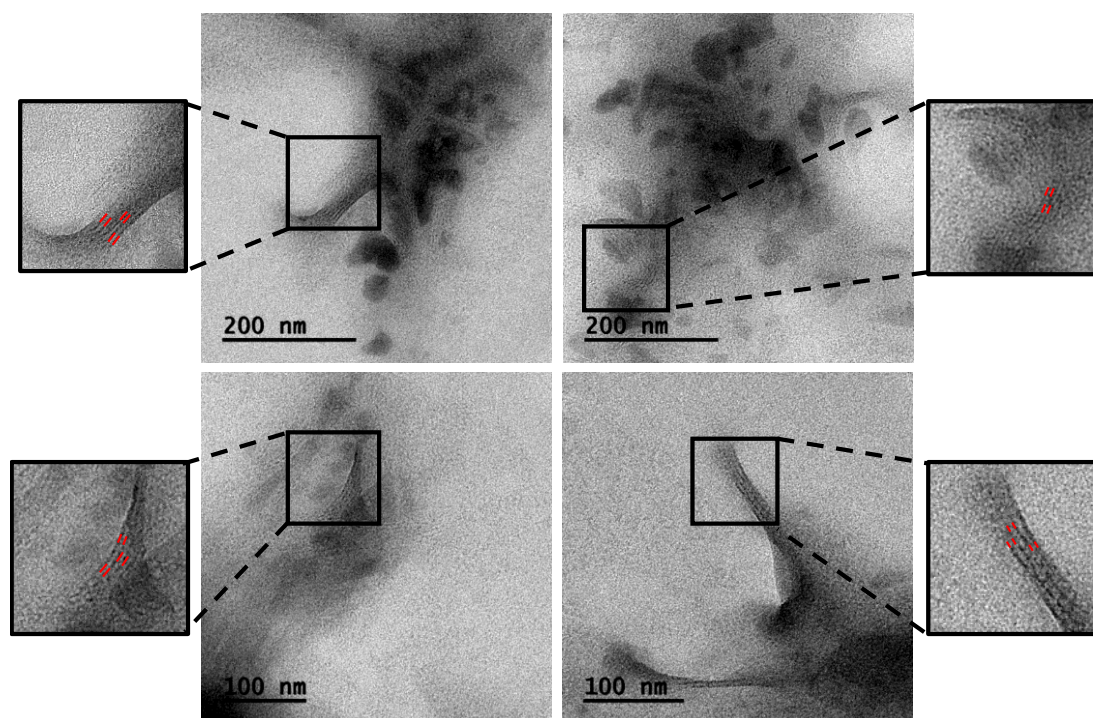


Figure S1D. TEM images of the nanotubes formed by the self-assembly of compound **GC2** ($1.0 \cdot 10^{-5}$ M, $\text{H}_2\text{O}/\text{THF}$ 7:3) on C-formvar Cu grids. Measured nanotube width: ~ 5 nm.

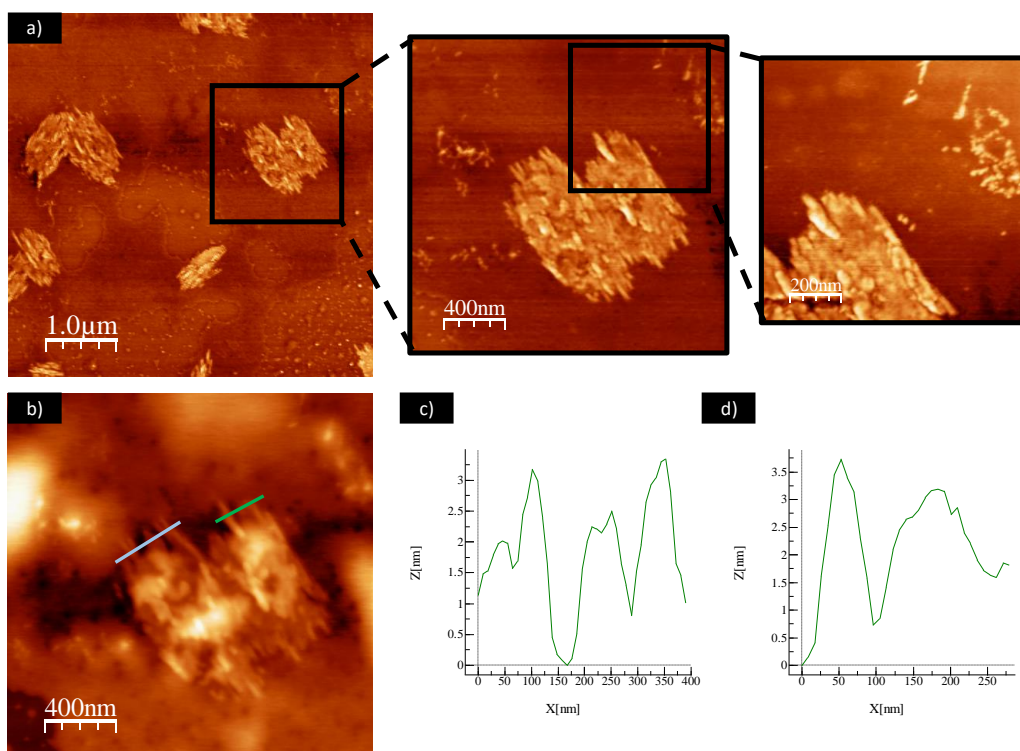


Figure S1E. Phase (a and zooms in a) and height (b) AFM images of the aggregates formed by the self-assembly of compound **GC3** ($1.0 \cdot 10^{-7}$ M, H_2O) on mica. Height profile of the aggregates along the grey (c) and green lines (d).

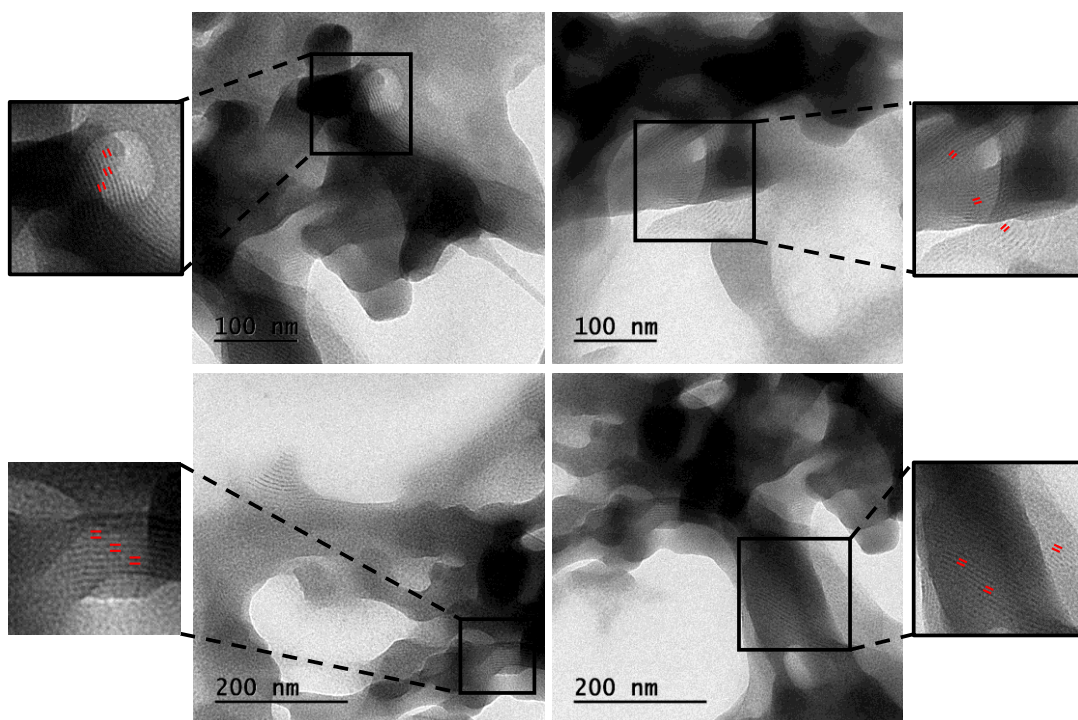


Figure S1F. TEM images of the nanotubes formed by the self-assembly of compound **GC3** ($1.0 \cdot 10^{-6}$ M, H_2O) on C-formvar Cu grids. Measured nanotube width: ~ 6 nm.

S2. Study of the effect of the Temperature on the Supramolecular Aggregation

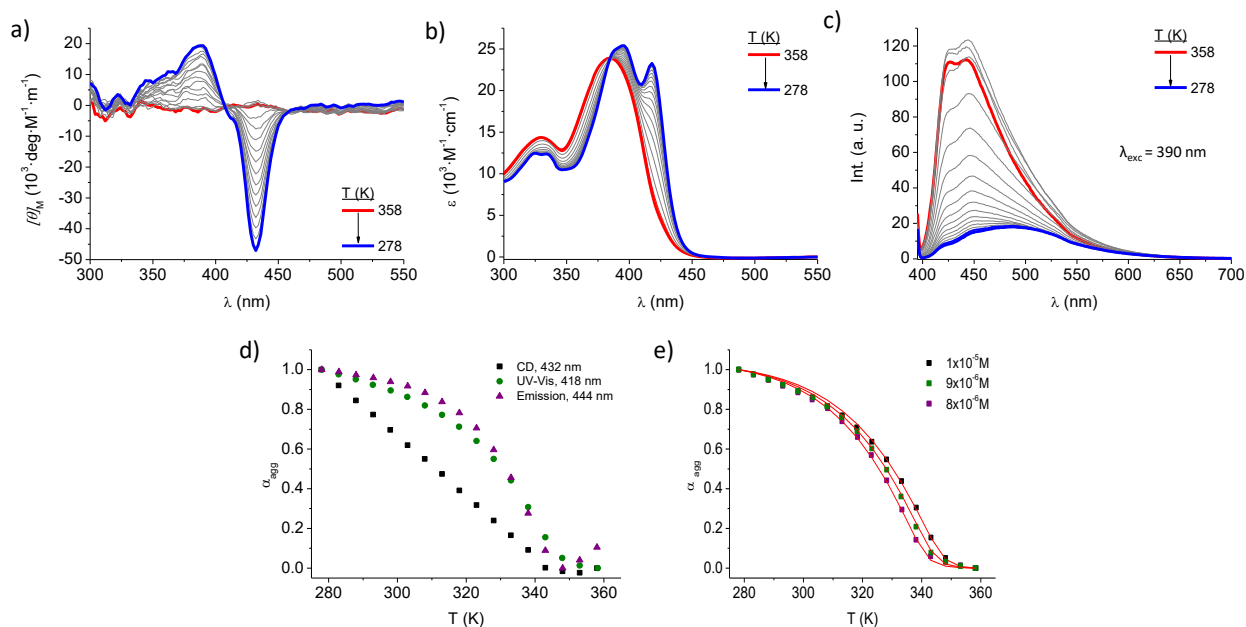


Figure S2A. Temperature-dependent CD (a), UV (b) and emission (c) experiments of compound **GC1** in H₂O ($l = 1$ cm) at $1.0 \cdot 10^{-5}$ M. Comparison of the spectroscopic changes at selected wavelengths in each technique (d) and curves obtained from the UV-vis data at 418 nm at 3 concentrations and fitted to the corresponding nucleation-elongation models (red lines).⁷

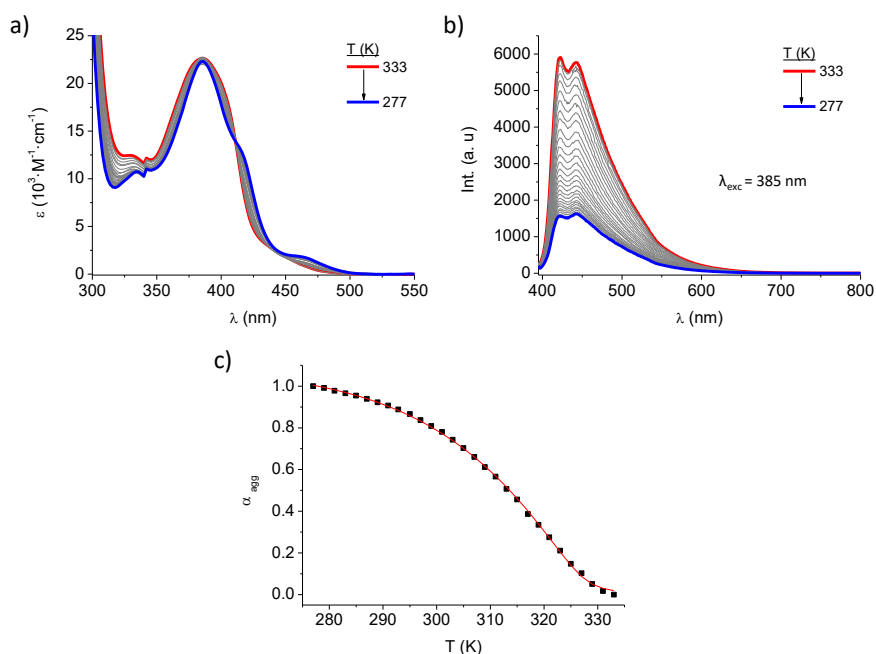


Figure S2B. Temperature-dependent UV-vis (a) and emission (b) experiments of compound **GC2** in H₂O/THF 9/1 ($l = 1$ cm) at $1.0 \cdot 10^{-5}$ M. Curve (c) obtained from the emission data at 422 nm and fitted to the corresponding nucleation-elongation model (red line).⁷

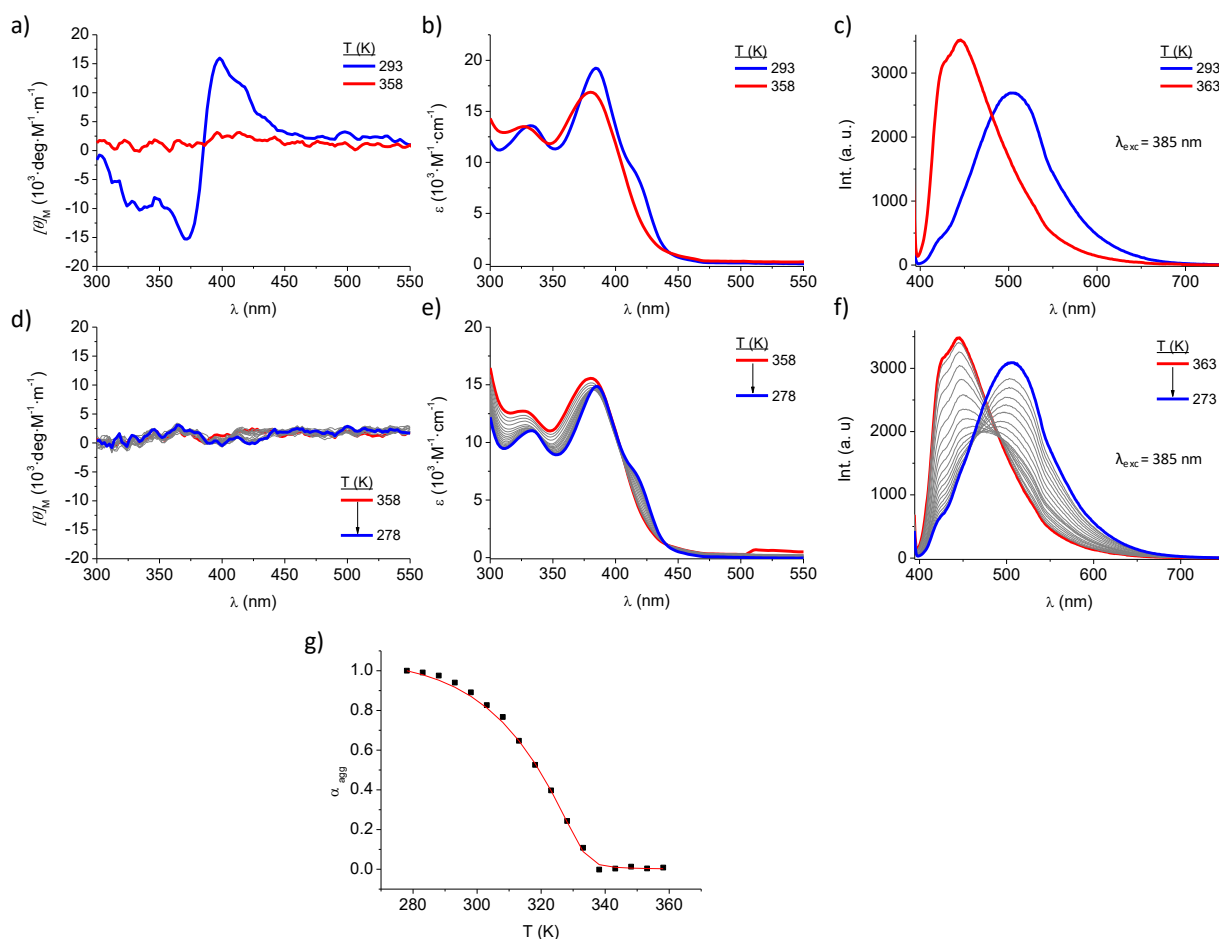


Figure S2C. CD (left), UV-vis (middle) and emission (right) spectra of compound **GC3** in H₂O ($l = 1$ cm) at $1.0 \cdot 10^{-5}$ M at 293 K and 358 K (a-c), temperature-dependent spectra obtained upon cooling after heating the sample at 358 K for 30 min (d-f) and temperature-dependent curve from the absorption data at 444 nm and fitted to the corresponding nucleation-elongation model (red line).⁷

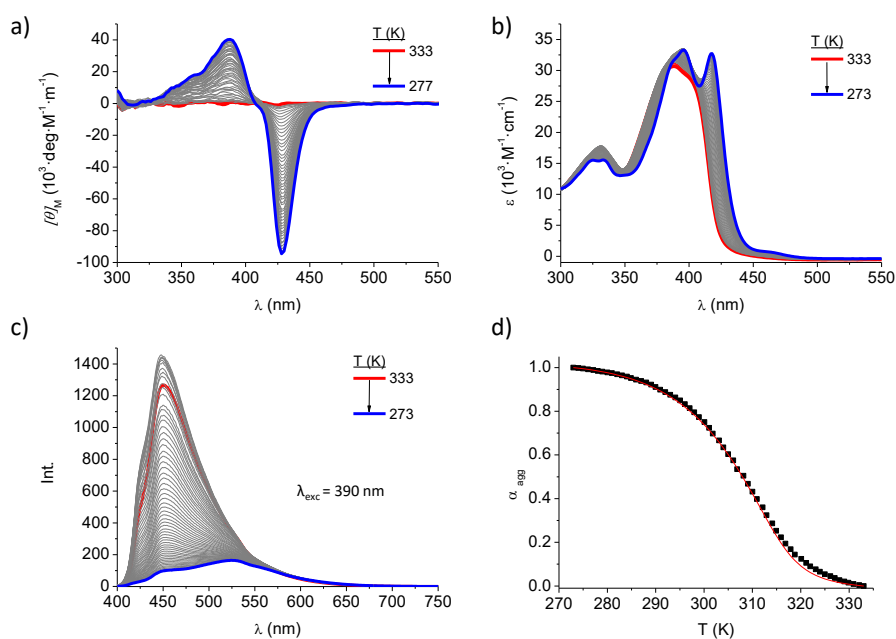


Figure S2D. Temperature-dependent CD (a), UV (b) and emission (c) experiments of compound **GC1** in H₂O/THF 8/2 ($l = 1$ mm) at $2.0 \cdot 10^{-4}$ M. Curve (d) obtained from the UV-Vis data at 418 nm and fitted to the corresponding nucleation-elongation model (red line).⁷

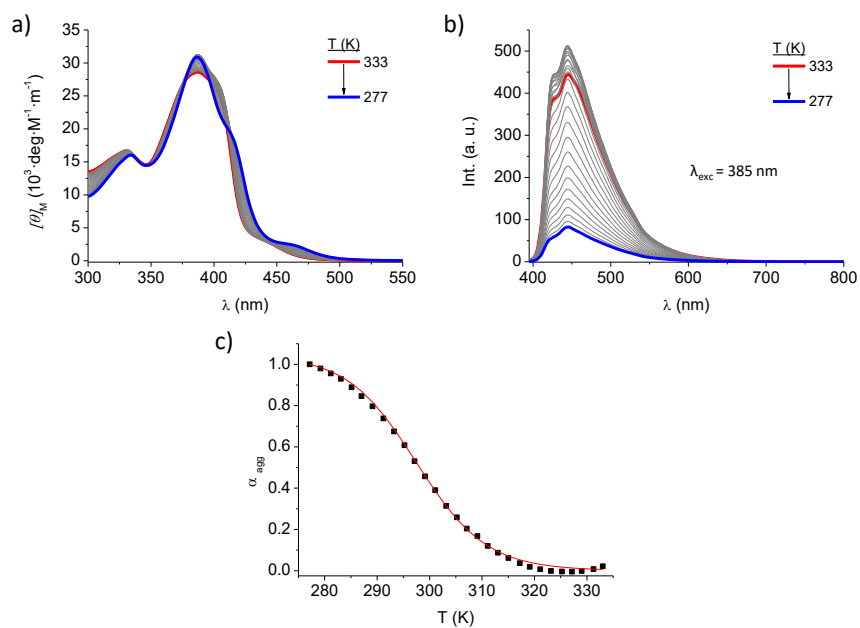


Figure S2E. Temperature-dependent UV-vis (a) and emission (b) experiments of compound **GC2** in H₂O/THF 8/2 (*l* = 1mm) at 5.0·10⁻⁵ M. Curve (c) obtained from the UV-Vis data at 424 nm and fitted to the corresponding nucleation-elongation model (red line).⁷

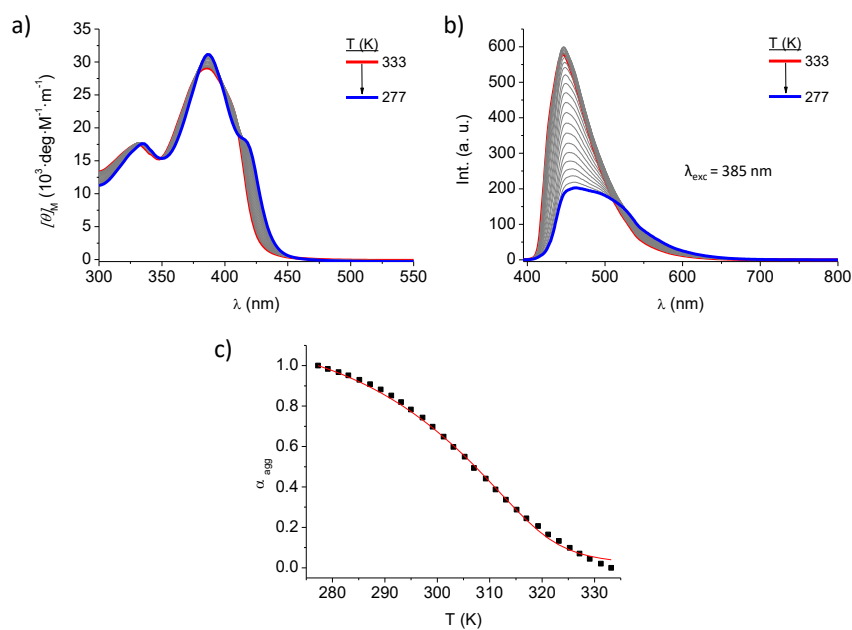


Figure S2F. Temperature-dependent UV-vis (a) and emission (b) experiments of compound **GC3** in H₂O/THF 8/2 (*l* = 1mm) at 2.0·10⁻⁴ M. Curve (c) obtained from the UV-Vis data data at 420 nm and fitted to the corresponding nucleation-elongation model (red line).⁷

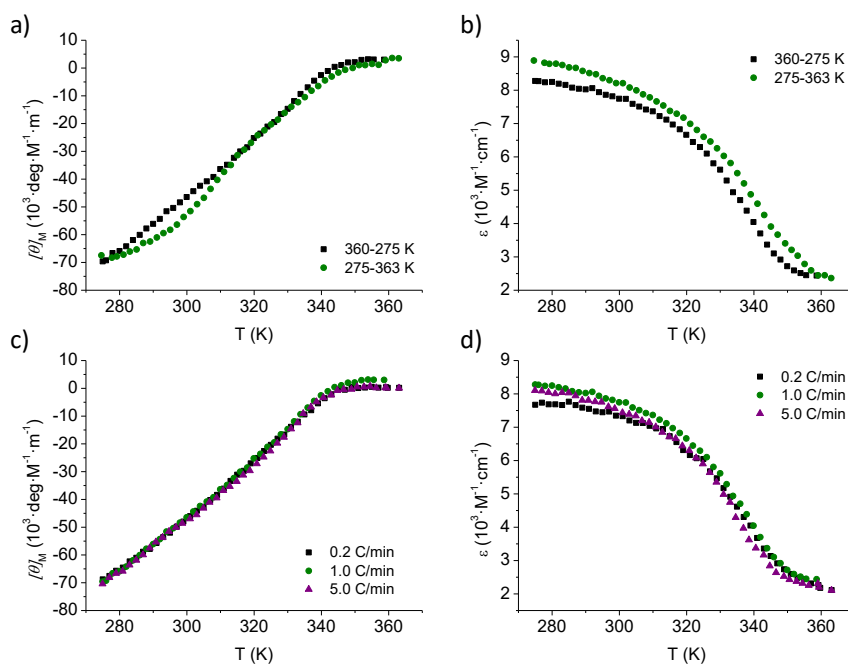


Figure S2G. Comparison of cooling and heating trends (a,b) and cooling trends at different cooling rates (c, d) by CD (a, c) and UV-vis (b, d) of compound **GC1** in H_2O ($l = 1\text{cm}$) at $1.0 \cdot 10^{-5} \text{ M}$ at 426 nm .

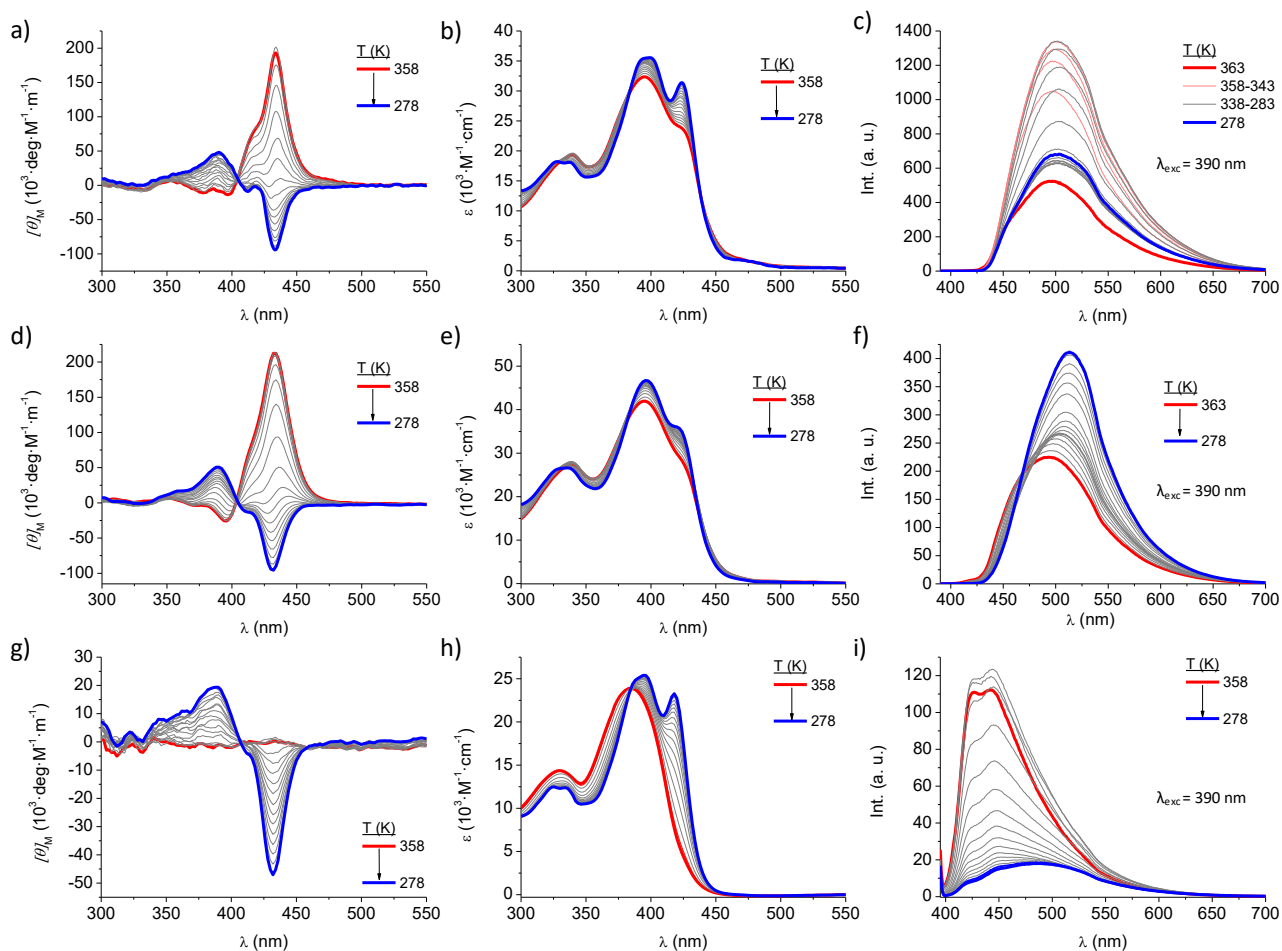


Figure S2H. Temperature-dependent CD (left), UV-vis (middle), and Emission (right) spectra of compound **GC1** in H_2O at $3.0 \cdot 10^{-4} \text{ M}$ (a-c), $1.0 \cdot 10^{-4} \text{ M}$ (d-f) and $1.0 \cdot 10^{-5} \text{ M}$ (g-i).

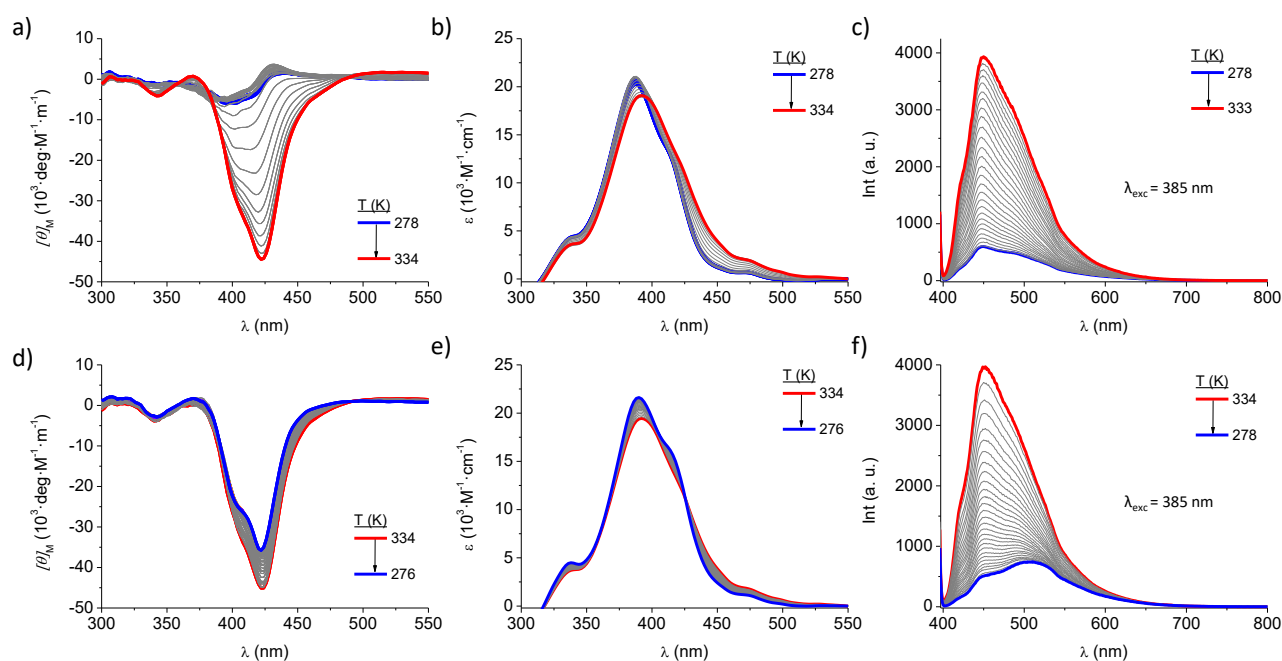


Figure S2I. CD (left), UV-vis (middle) and emission (right) heating (a-c) and cooling (d-f) experiments of compound **GC2** in H₂O (*l* = 1cm) at 1.0·10⁻⁴ M.

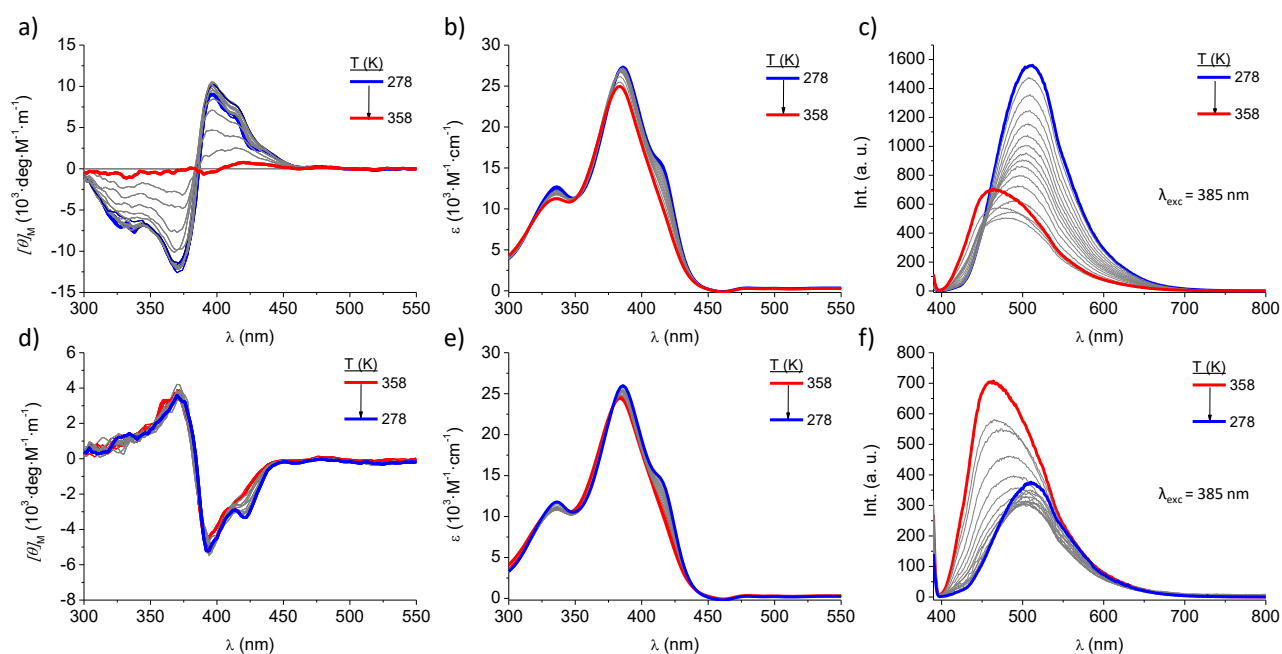


Figure S2J. CD (left), UV-vis (middle) and Emission (right) heating (a-c) and cooling (d-f) experiments of compound **GC3** in H₂O (*l* = 1cm) at 1.0·10⁻⁴ M. When the heating/cooling experiments are performed on **GC3** at 1.0·10⁻⁴ M, the formation of the dehydrated aggregated is not detected in the heating experiment and is only achieved when the sample remains at high temperature for more than 5 minutes and, as previously, this signal keeps almost invariable during the cooling experiment.

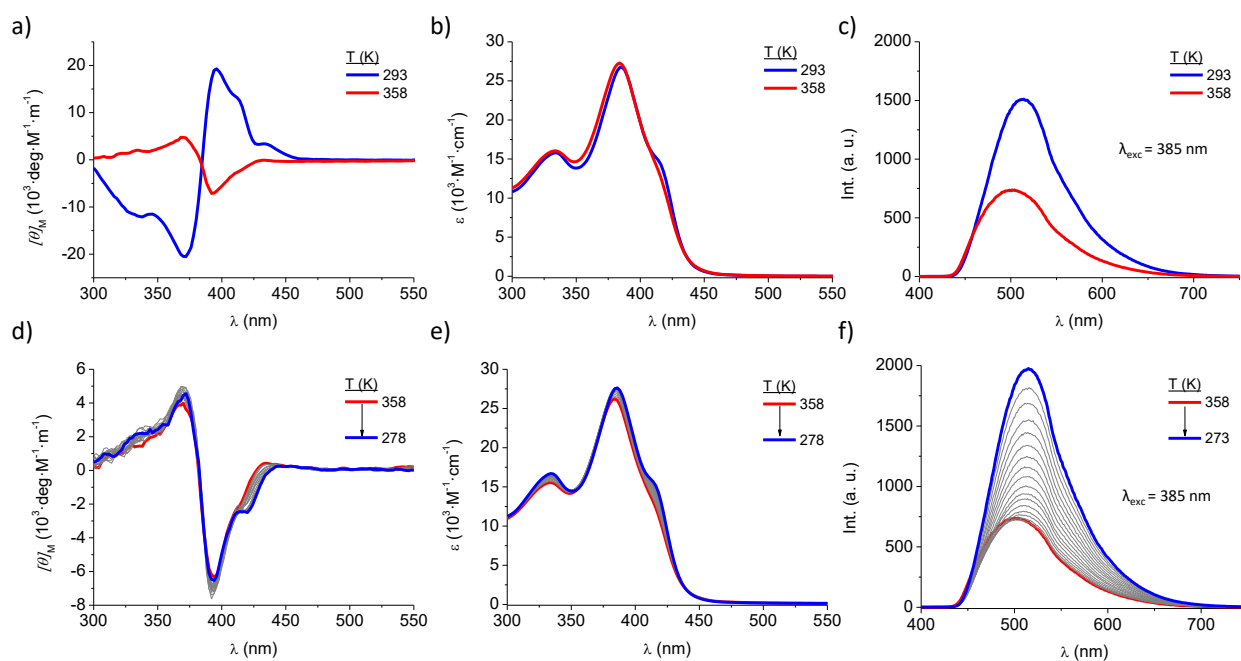


Figure S2K. CD (left), UV-vis (middle) and Emission (right) spectra of compound **GC3** in H₂O ($l = 1\text{ cm}$) at $1.0 \cdot 10^{-3}\text{ M}$ at 293 K and 358 K (a-c), temperature-dependent experiments after heating the sample at 358 K for 30 min (d-f) and corresponding cooling curves at different wavelengths (g-h).

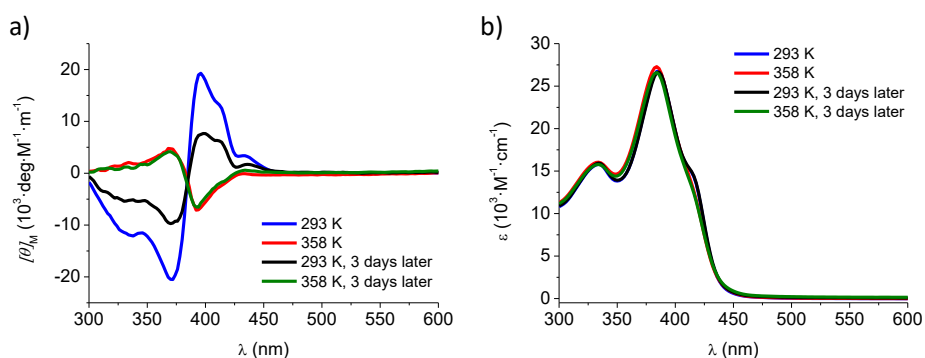


Figure S2L. Evolution of the signal found for compound **GC3** at $1.0 \cdot 10^{-3}\text{ M}$ in H₂O ($l = 1\text{ cm}$) with temperature and time by CD (a) and UV-vis (b).

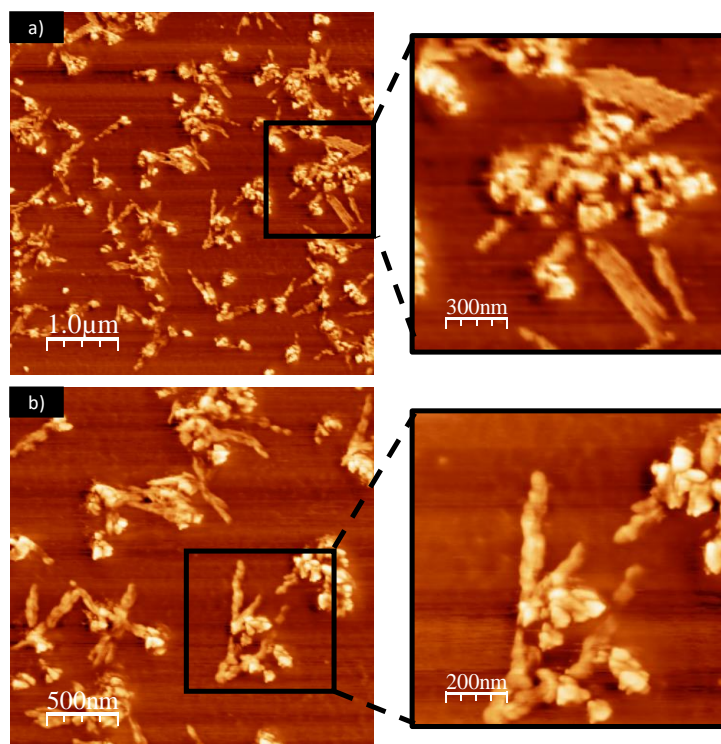


Figure S2M. Phase AFM images of the aggregates formed by the self-assembly of compound **GC1** at high concentration ($5.0 \cdot 10^{-5}$ M) and high temperature in H_2O on HOPG.

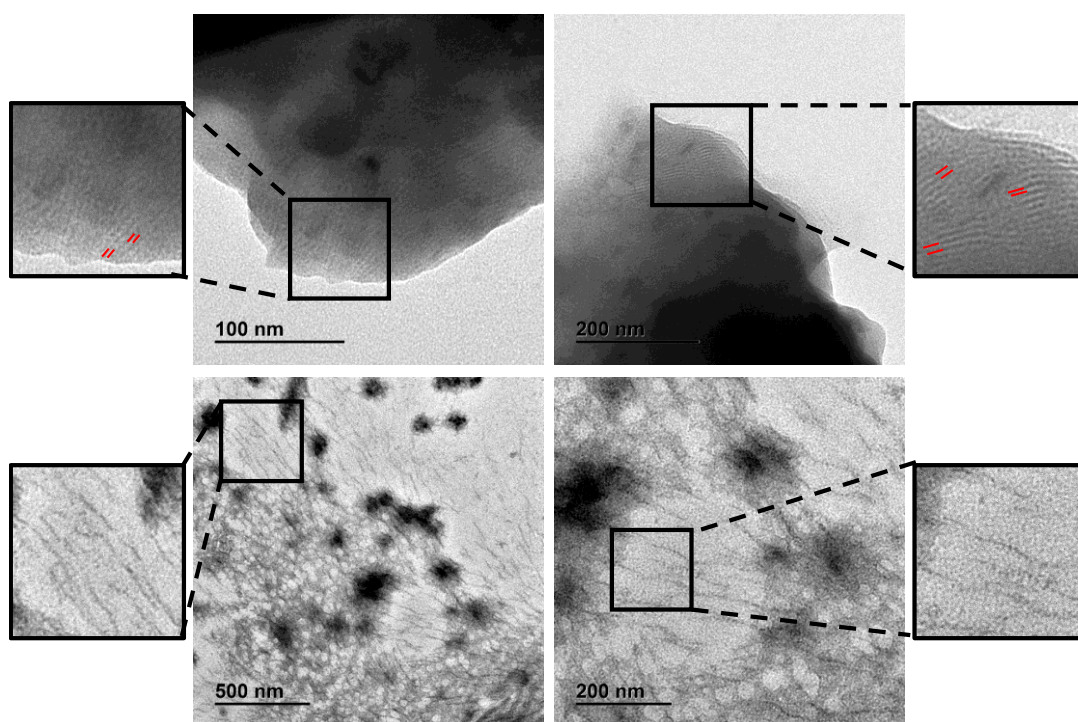


Figure S2N. TEM images of compound **GC1** at high concentration ($5.0 \cdot 10^{-5}$ M) and high temperature in H_2O on C-formvar Cu grids. Some areas maintained the tubular features observed at room temperature (top images; measured nanotube width: ~ 5 nm) and in some other areas ill-defined objects and thin fibers were imaged (bottom images).

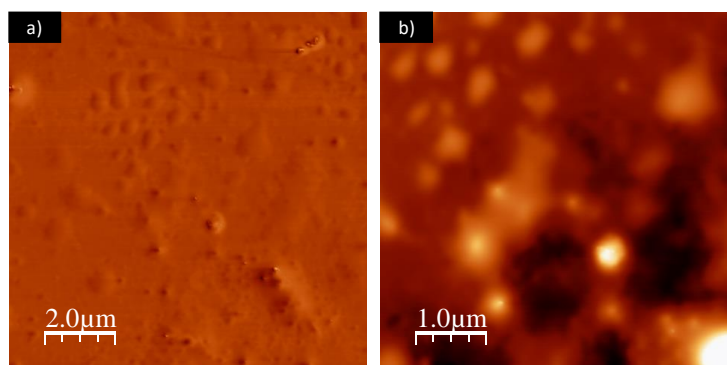


Figure S2O. Phase (a) and height (b) AFM images of the circular objects formed by the self-assembly of compound **GC3** at high concentration ($5.0 \cdot 10^{-5}$ M) and high temperature in H₂O on mica.

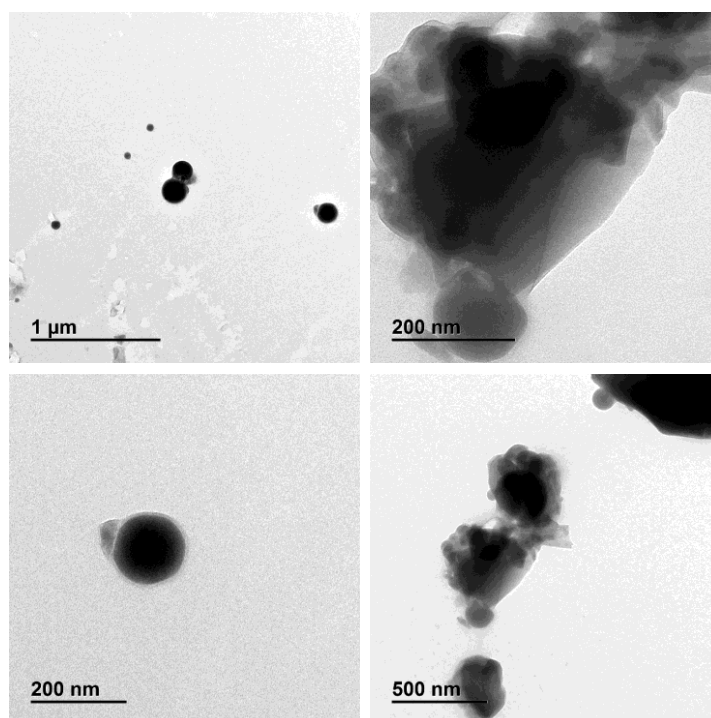


Figure S2P. TEM images of the circular objects formed by the self-assembly of compound **GC3** at high concentration ($5.0 \cdot 10^{-5}$ M) and high temperature in H₂O on C-formvar Cu grids.

S3. Study of the effect of the Solvent on the Supramolecular Aggregation

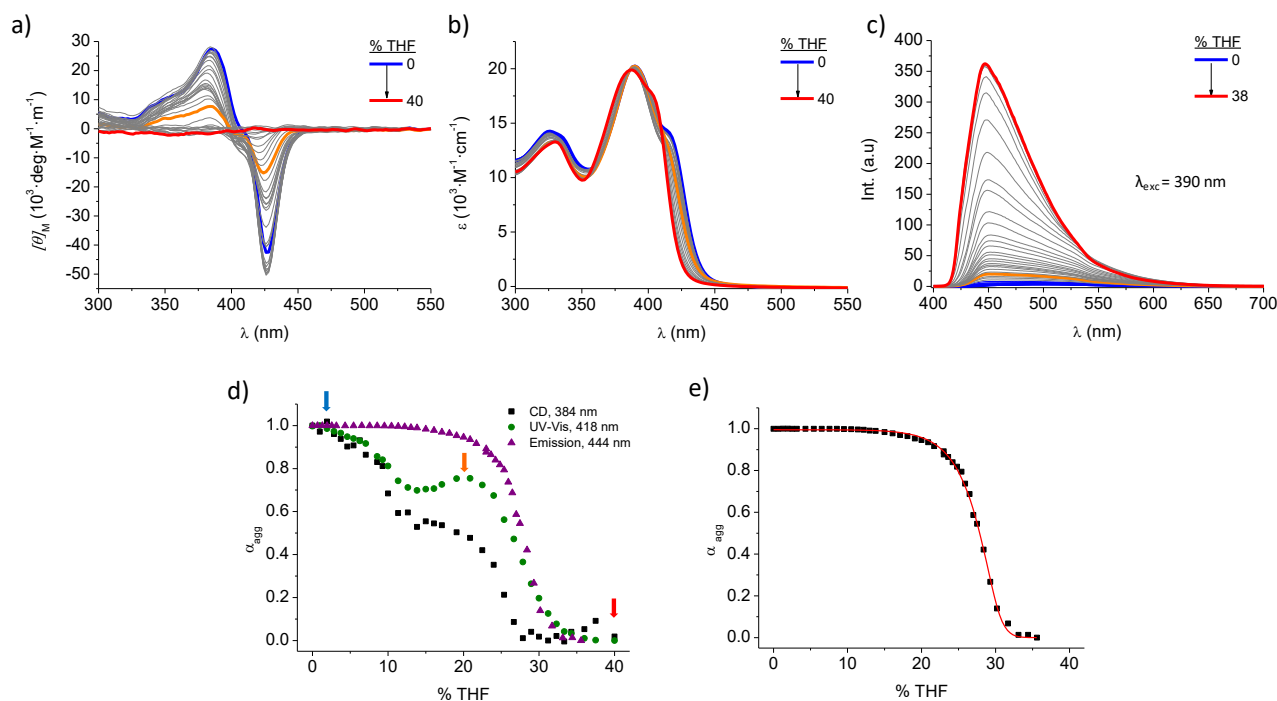


Figure S3A. (a) CD, (b) absorption and (c) emission spectral changes recorded for **GC1** as a function of solvent composition in H₂O-THF mixtures (at 298 K; 2.0·10⁻⁴ M). (d) Spectroscopic trends recorded at specific wavelengths in a-c. (e) solvent-dependent curve from the emission data at 444 nm and fitting to a solvent-dependent nucleation-elongation model (red line).⁸

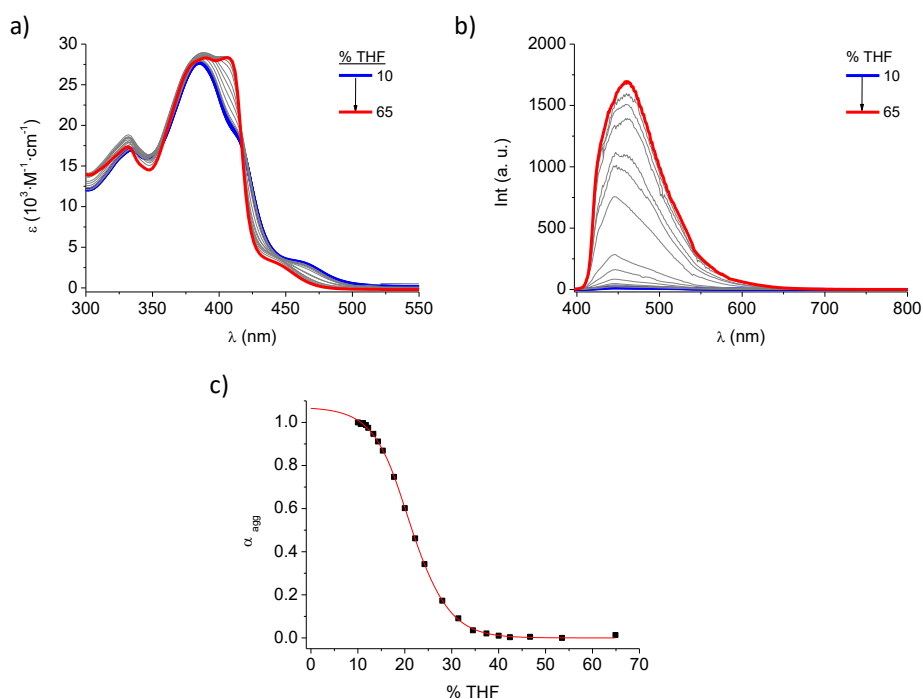


Figure S3B. Changes in spectroscopic features of compound **GC2** as a function of solvent composition in H₂O-THF mixtures (at 298 K; 1.0·10⁻⁴ M), by UV-vis (a) and Fluorescence (b) spectroscopies. Solvent-dependent curve from the absorption data at 408 nm and fitting to a solvent-dependent nucleation-elongation model (red line).⁸ Because of the lack of solubility of this compound in pure H₂O, its corresponding 0% THF experiment is not shown in the Figure.

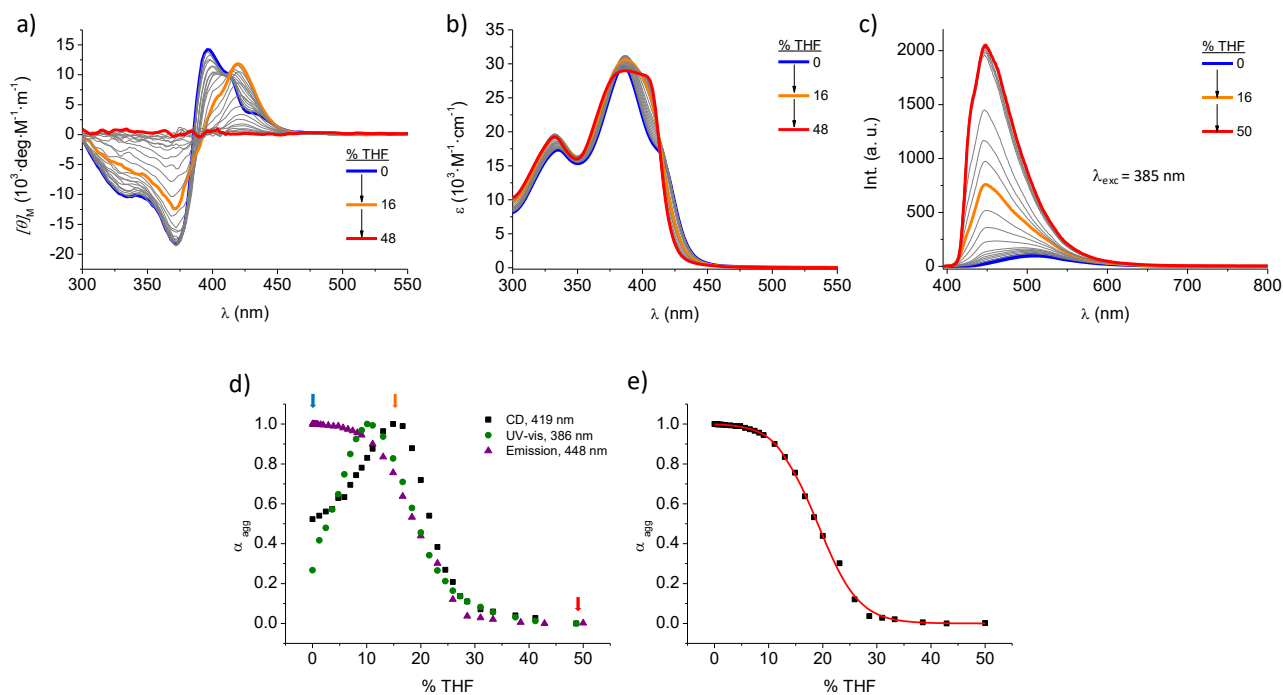


Figure S3C. (a) CD, (b) absorption and (c) emission spectral changes recorded for **GC3** as a function of solvent composition in H₂O-THF mixtures (at 298 K; 1.0·10⁻⁴ M). (d) Spectroscopic trends recorded at specific wavelengths in a-c. (e) solvent-dependent curve from the emission data at 448 nm and fitting to a solvent-dependent nucleation-elongation model (red line).⁸

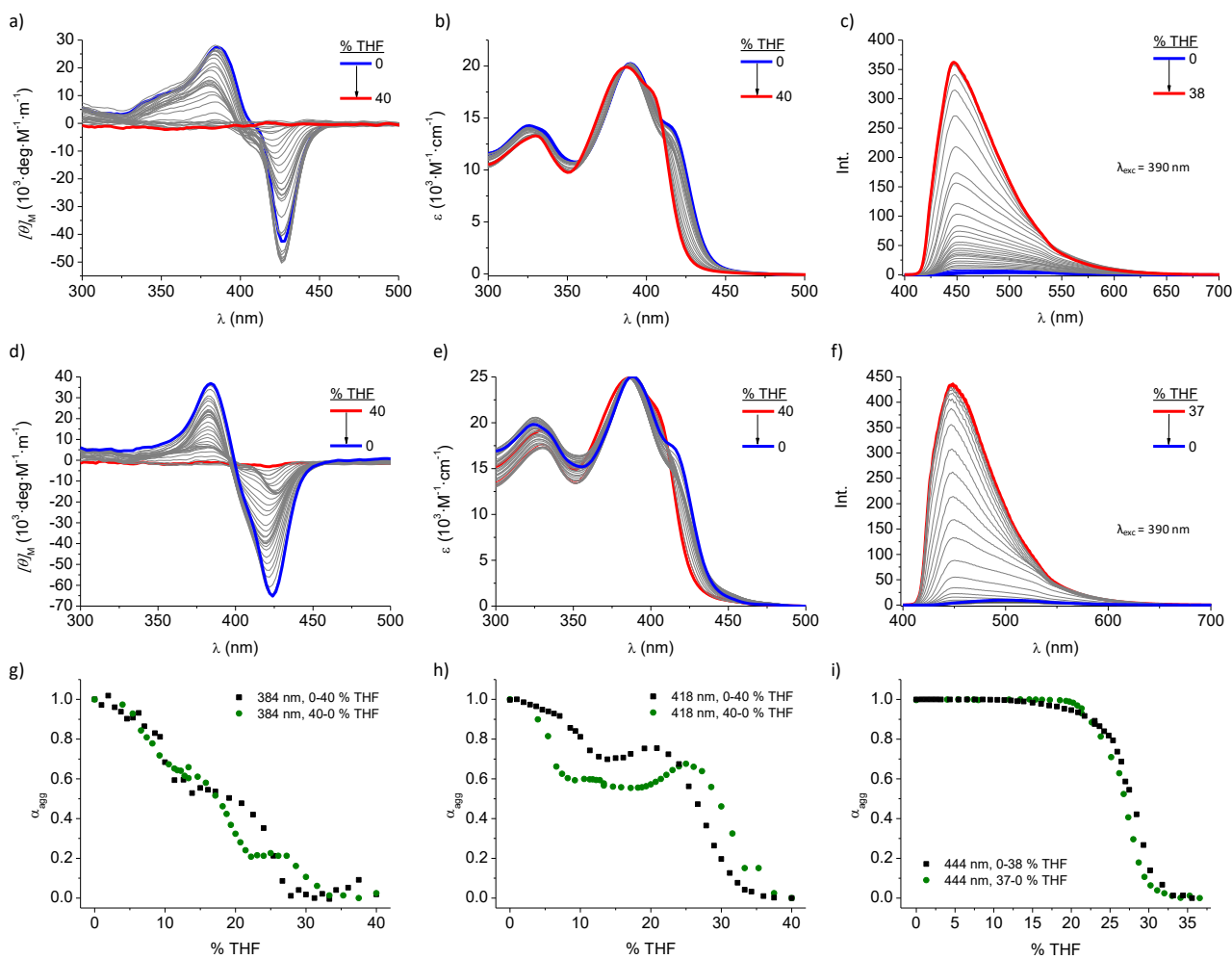


Figure S3D. Solvent-dependent CD (a and d), UV (b and e) and emission (c and f) experiments of compound **GC1** in H₂O/THF mixtures ($l = 1\text{cm}$) at $2.0 \cdot 10^{-4}\text{ M}$. Figures a), b) and c) correspond to *depolymerization* studies (increasing V_{THF} ; black points), and d), e) and f) to *polymerization* studies (decreasing V_{THF} ; green points). Comparison of the spectroscopic changes at selected wavelengths in each technique for both, depolymerization and polymerization experiments.

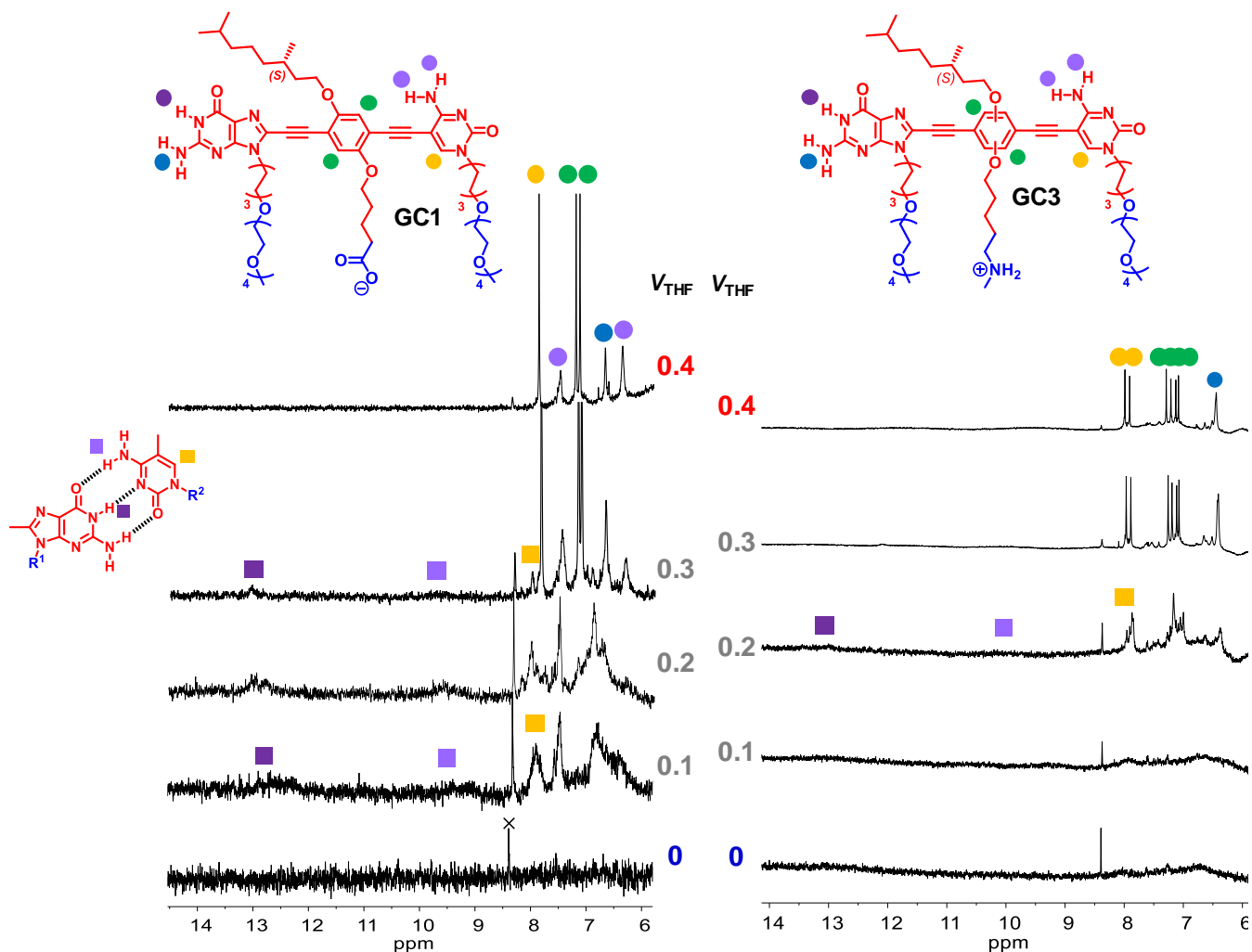


Figure S3E. Structure of compound **GC1** and **GC3** and ¹H NMR spectra acquired at different H₂O:THF-D₈ compositions of **GC1** ($2.0 \cdot 10^{-4}\text{ M}$) and **GC3** ($1.0 \cdot 10^{-3}\text{ M}$). Circles and squares indicate respectively protons in the monomer and aggregated forms.

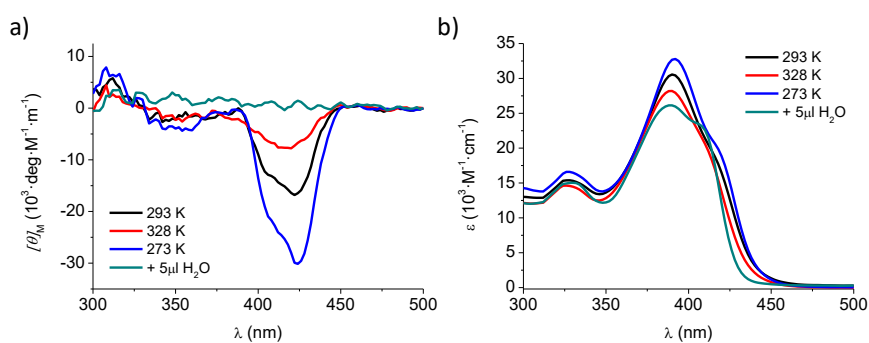


Figure S3F. (a) CD, (b) absorption spectra of **GC2** in THF at $1.0 \cdot 10^{-4}\text{ M}$ at different temperatures and with the addition of H₂O.

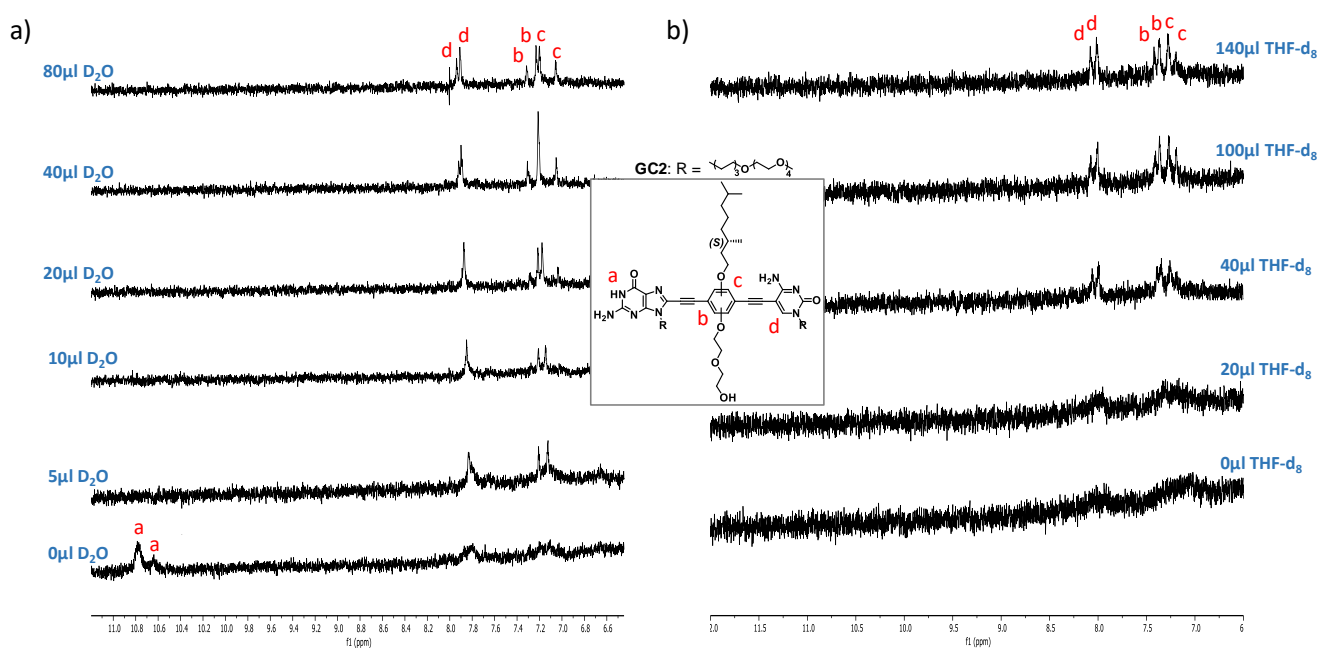


Figure S3G. Partial ^1H NMR (300 MHz, 298 K, $1.0 \cdot 10^{-3}$ M) spectra of compound **GC2** in THF-d_8 with increasing amounts of D_2O (a) and in $\text{D}_2\text{O}/\text{THF-d}_8$ 8/2 with increasing amounts of THF-d_8 (b). Every ^1H presents two signals that correspond to both possible regioisomers.

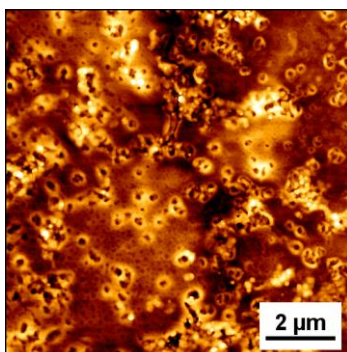


Figure S3H. Phase AFM images of the circular objects formed by the self-assembly of compound **GC2** ($1.0 \cdot 10^{-4}$ M, $\text{H}_2\text{O}/\text{THF}$ 7/3) on HOPG.

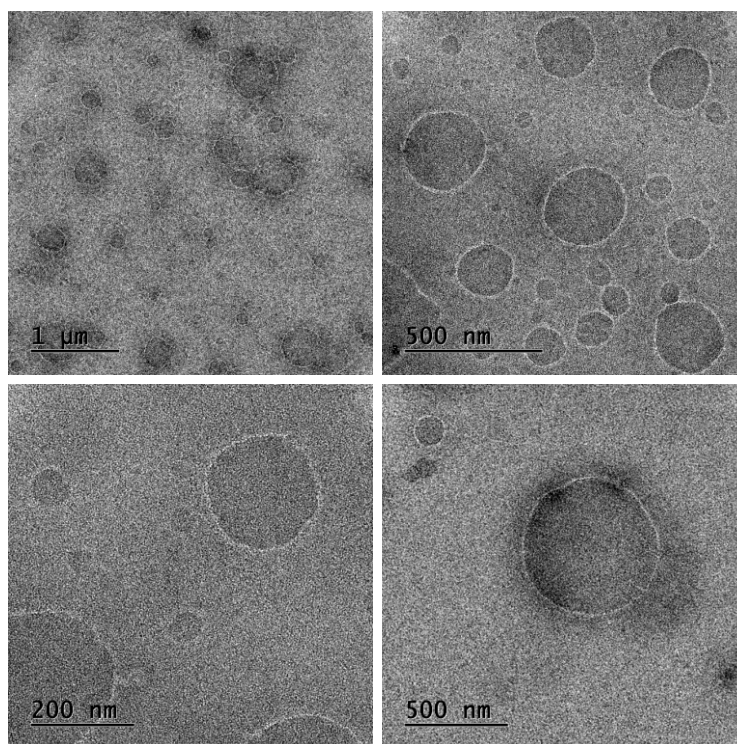


Figure S3I. TEM images of the circular objects formed by the self-assembly of compound **GC2** ($1.0 \cdot 10^{-6}$ M, THF) on Carbon-Cu grids.

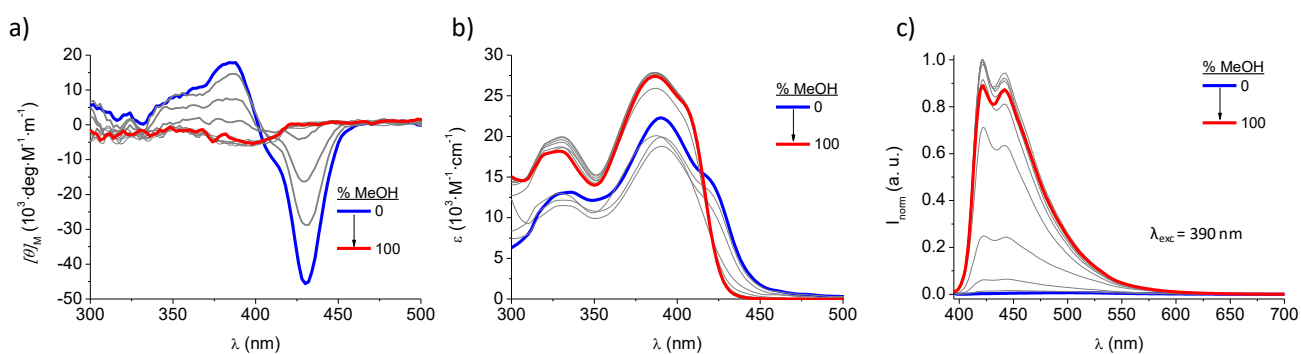


Figure S3J. Changes in spectroscopic features of compound **GC1** as a function of the volume fraction of MeOH in water by CD (a), UV-vis (b) and fluorescence (c) spectroscopies. All the experiments were carried out at $1.0 \cdot 10^{-5}$ M, 293K, $l = 1$ cm.

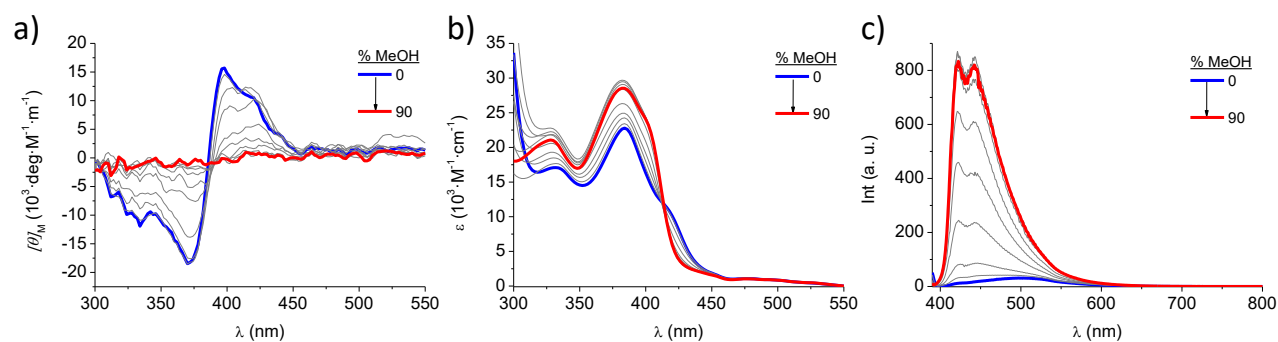


Figure S3K. Changes in spectroscopic features of compound **GC3** as a function of the volume fraction of MeOH in water by CD (a), UV-vis (b) and fluorescence (c) spectroscopies. All the experiments were carried out at $1.0 \cdot 10^{-5}$ M, 293K, $l = 1$ cm.

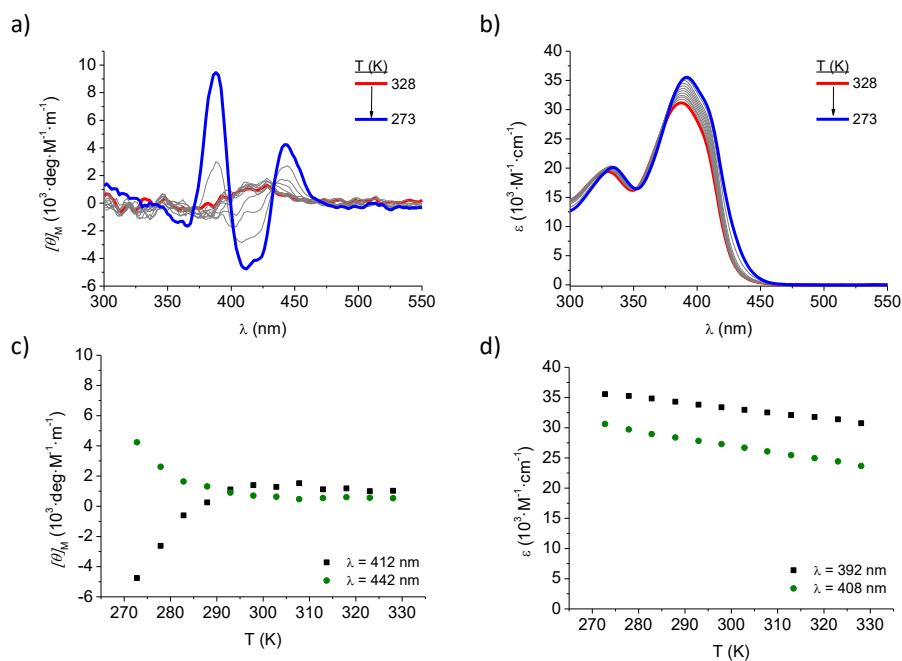


Figure S3L. Temperature-dependent CD (a) and UV-Vis (b) experiments of compound **GC1** in MeOH ($l = 1\text{ mm}$) at $3.0 \cdot 10^{-4}\text{ M}$ and corresponding cooling curves at different wavelengths (c-d). CD signal was observed at temperatures below 20°C .

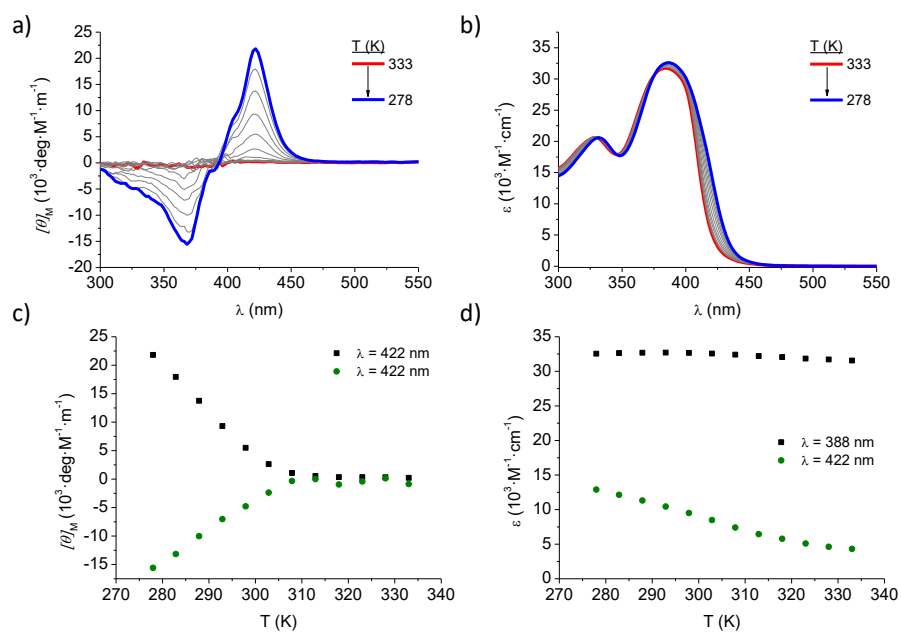


Figure S3M. Temperature-dependent CD (a) and UV-Vis (b) experiments of compound **GC3** in MeOH ($l = 1\text{ mm}$) at $1.0 \cdot 10^{-3}\text{ M}$ and corresponding cooling curves at different wavelengths (c-d).

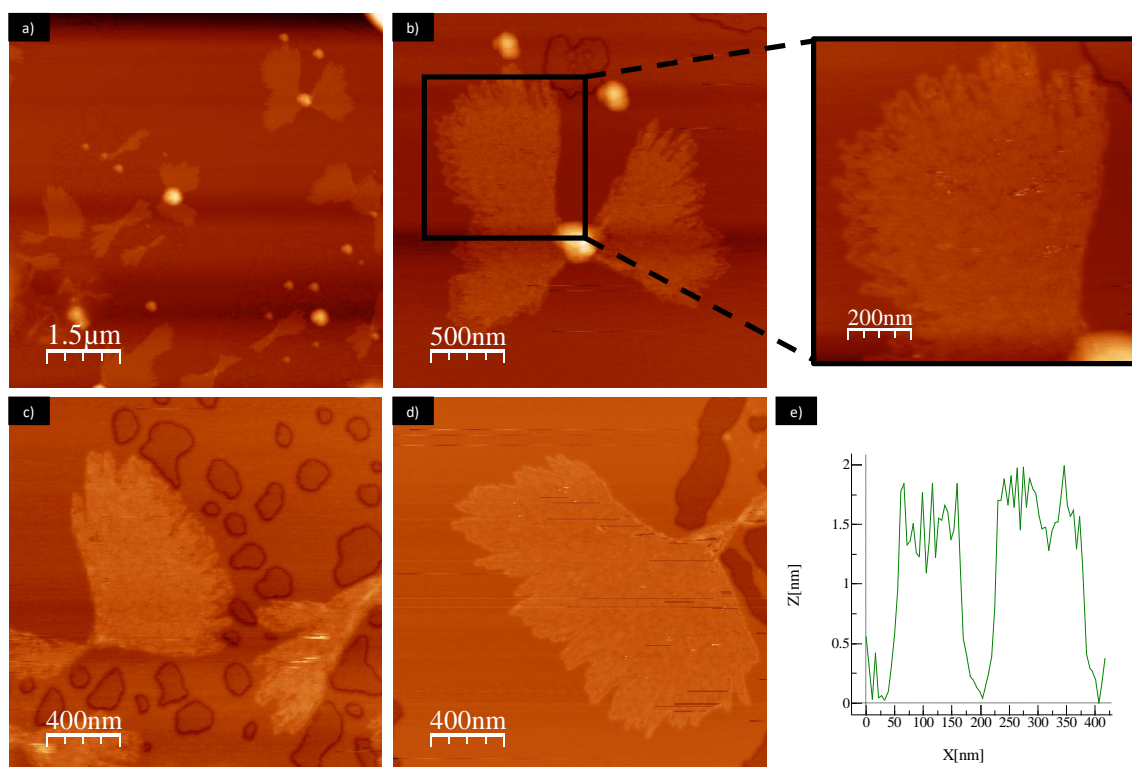


Figure S3N. Height AFM images (a-d and zoom in b) of the fibers of the gel formed by the self-assembly of compound **GC1** ($1.0 \cdot 10^{-6}$ M, MeOH) on mica surface and height profile (e) of the aggregates along the grey line in (d).

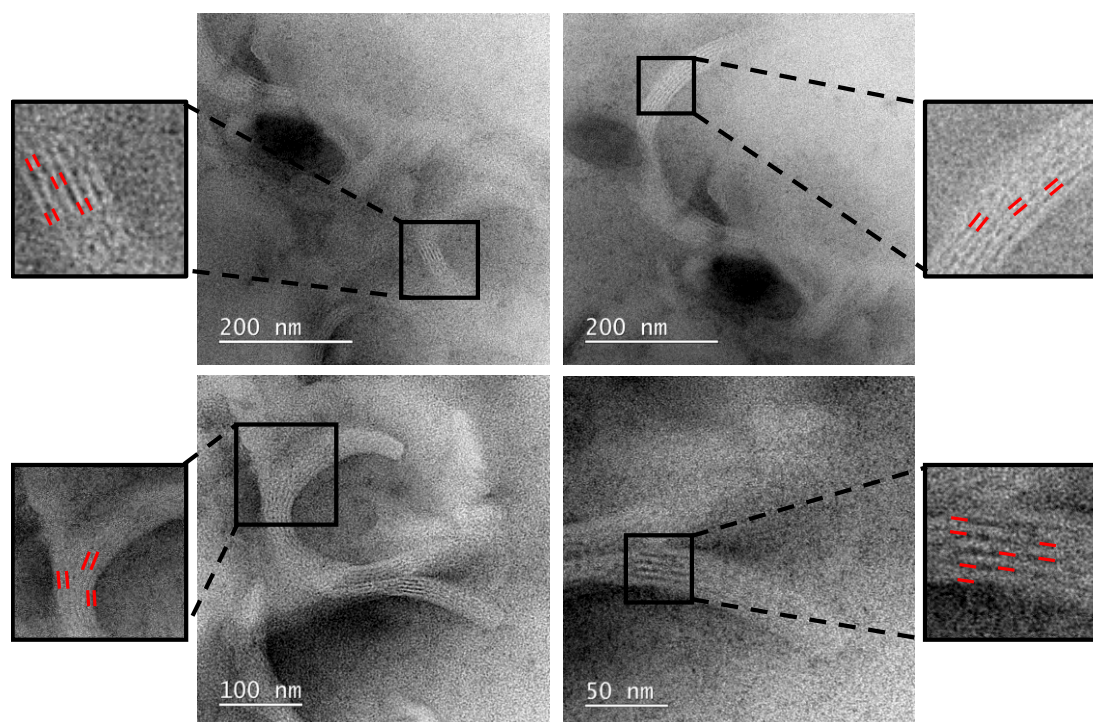


Figure S30. TEM images of the nanotubes formed by the self-assembly of compound **GC1** ($1.0 \cdot 10^{-5}$ M, MeOH) on C-formvar Cu grids. Measured nanotube width: ~ 6 nm.

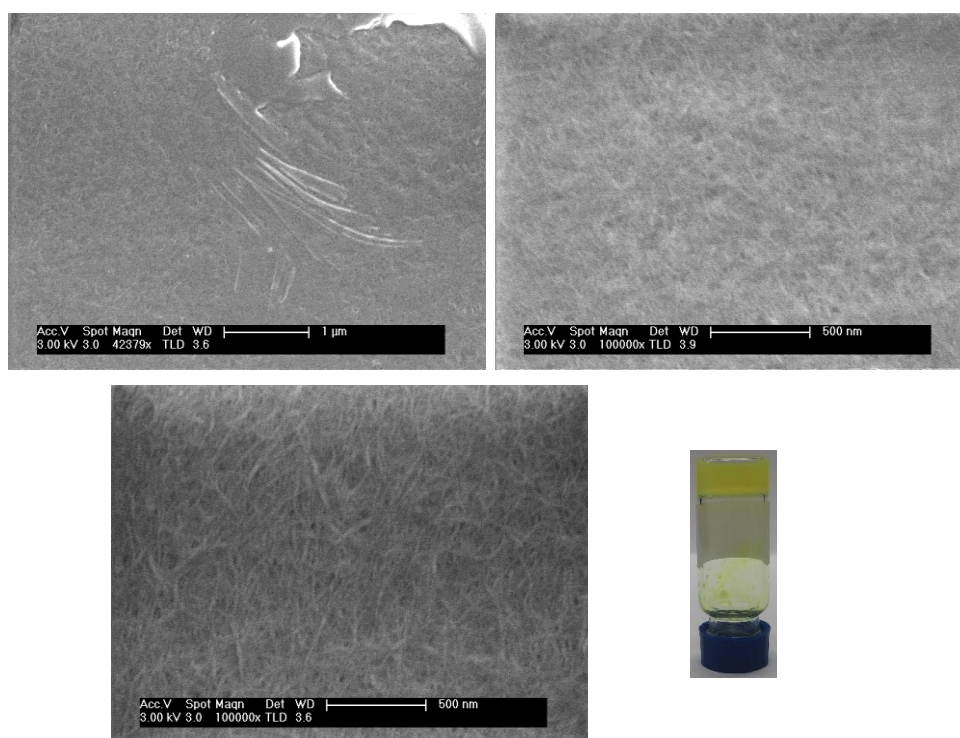


Figure S3P. SEM images of the fibers of the gel formed by the self-assembly of compound **GC1** ($7.0 \cdot 10^{-3}$ M, MeOH) on glass surface and picture of the gel formed in MeOH at 12mM.

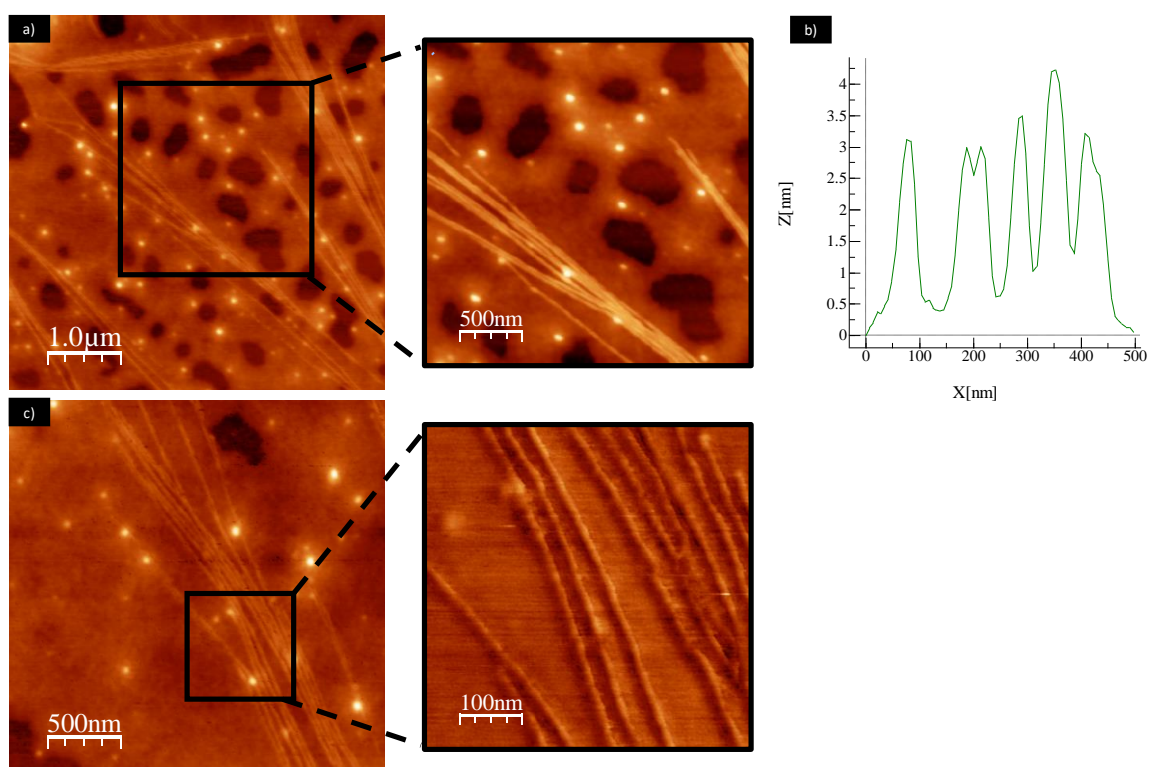


Figure S3Q. Height (a-c and zoom in a) and phase (zoom in c) AFM images of the fibers of the gel formed by the self-assembly of compound **GC3** ($1.0 \cdot 10^{-7}$ M, MeOH) on mica surface and height profile (b) of the aggregates along the grey line in zoom of (a).

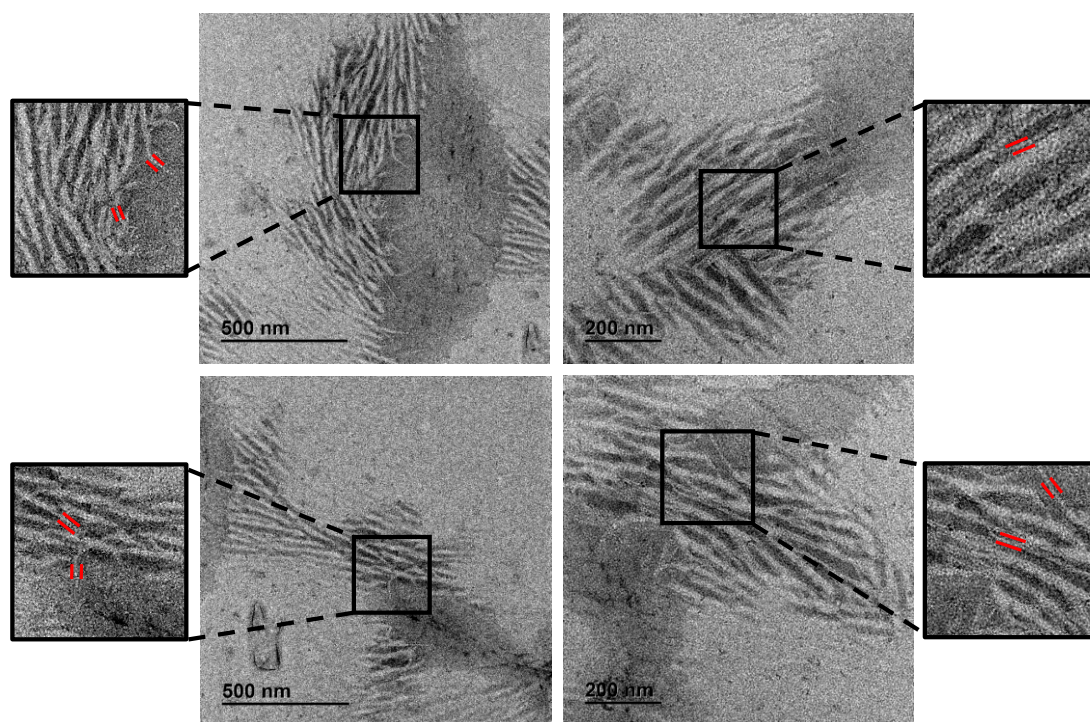


Figure S3R. TEM images of the nanotubes formed by the self-assembly of compound **GC3** ($5.0 \cdot 10^{-7}$ M, MeOH) on C-formvar Cu grids. Measured nanotube width: ~ 6 nm.

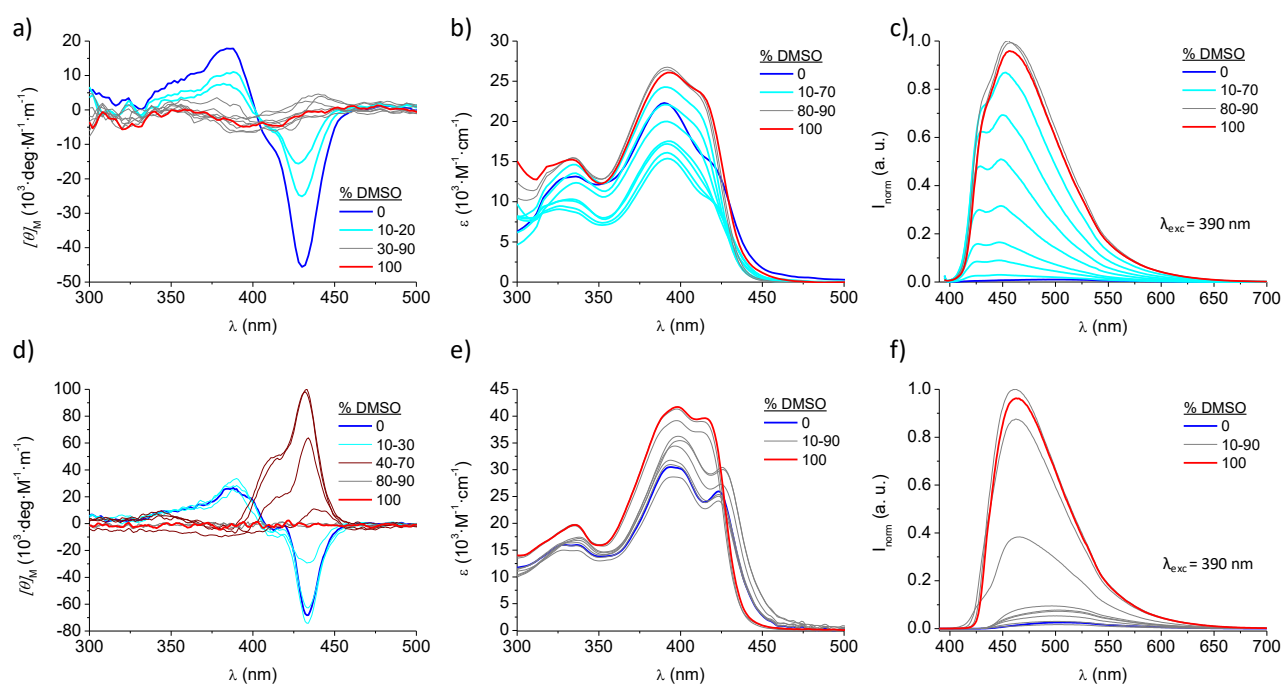


Figure S3S. Changes in spectroscopic features of compound **GC1** as a function of the volume fraction of DMSO in water by CD (left), UV-vis (middle) and fluorescence (right) spectroscopies at $1.0 \cdot 10^{-5}$ M (a-c) and $3.0 \cdot 10^{-4}$ M (d-f), 293K.

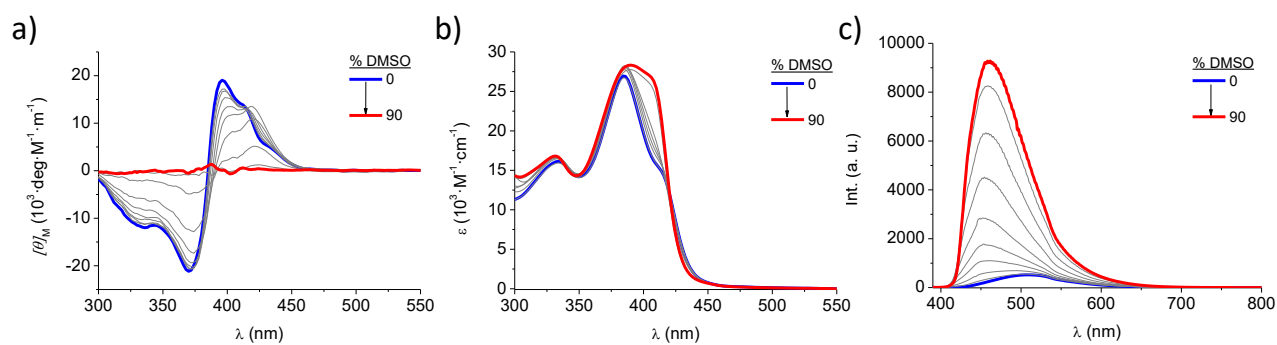


Figure S3T. Changes in spectroscopic features of compound **GC3** as a function of the volume fraction of DMSO in water by CD (a), UV-vis (b) and fluorescence (e) spectroscopies at $1.0 \cdot 10^{-4}$ M, 293 K.

S4. Study of the effect of the pH on the Supramolecular Aggregation

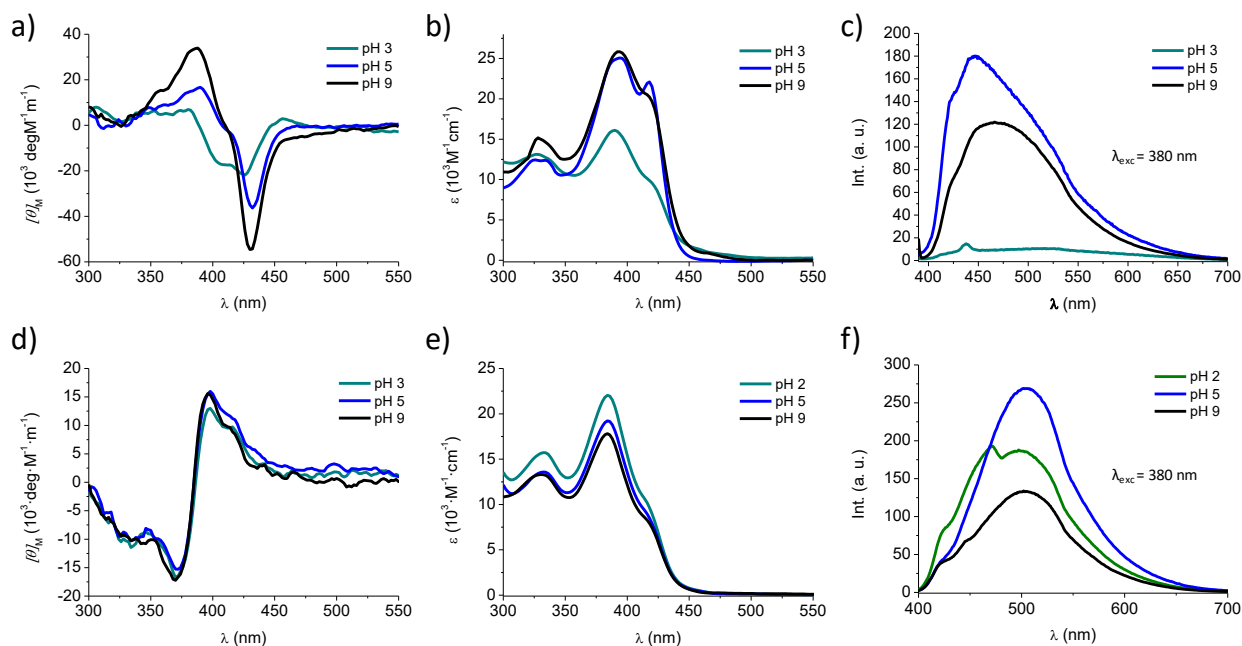


Figure S4A. Changes in spectroscopic features of compound **GC1** (a-c) and **GC3** (d-f) as a function of the pH in water by CD (left), UV-vis (middle) and fluorescence (right) spectroscopies. All the experiments were carried out at $1.0 \cdot 10^{-5}$ M, 293K, $l = 1$ cm.

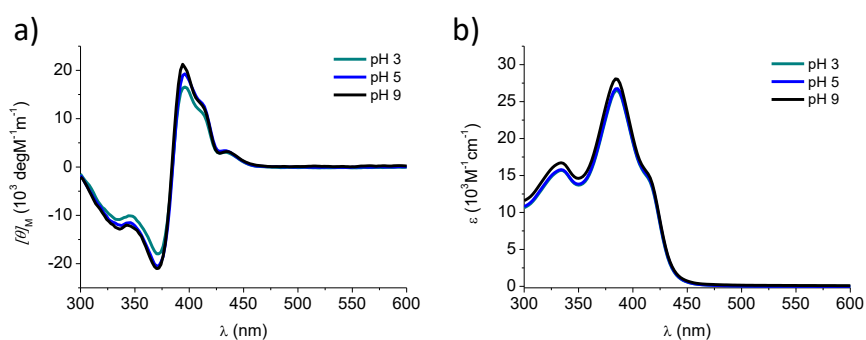


Figure S4B. Changes in spectroscopic features of compound **GC3** as a function of the pH in water by CD (a) and UV-vis (b) spectroscopies at $1.0 \cdot 10^{-3}$ M, 293K, $l = 1$ mm.

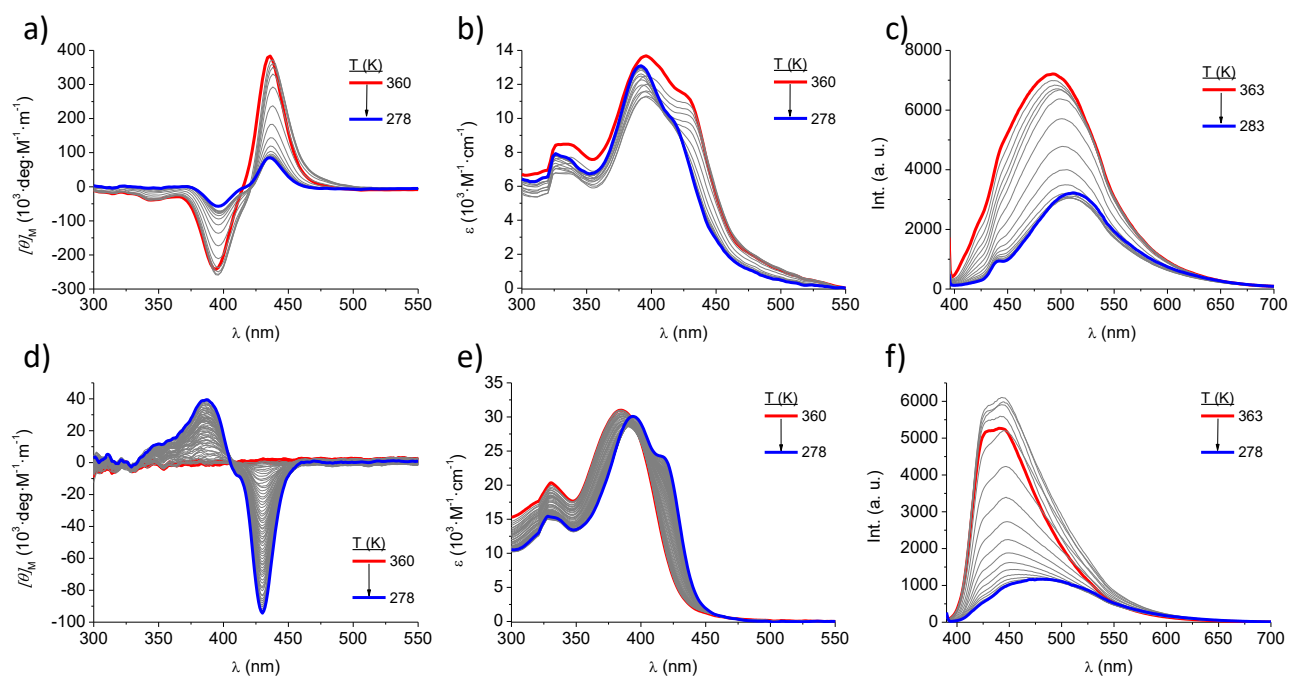


Figure S4C. Temperature-dependent CD (left), UV-vis (middle), and emission (right) spectra of compound **GC1** in H₂O, $1.0 \cdot 10^{-5}$ M at pH = 3, 1C/min (a-c) and pH = 9, 0.1C/min (d-f).

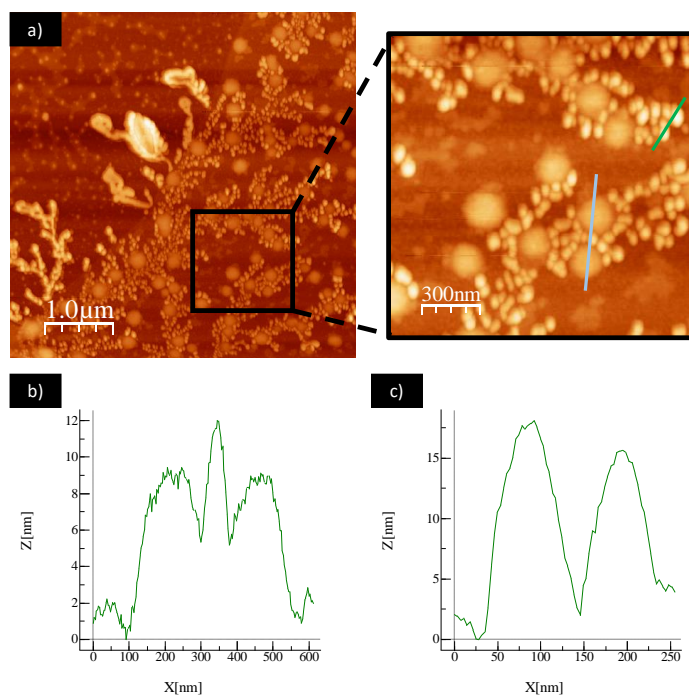


Figure S4D. Height (a and zoom in a) AFM images of the aggregates formed by the self-assembly of compound **GC1** ($1.0 \cdot 10^{-6}$ M, H₂O, pH 2) on mica. (b) and (c) Height profile of the aggregates along the blue and green line, respectively, in zoom in (a).

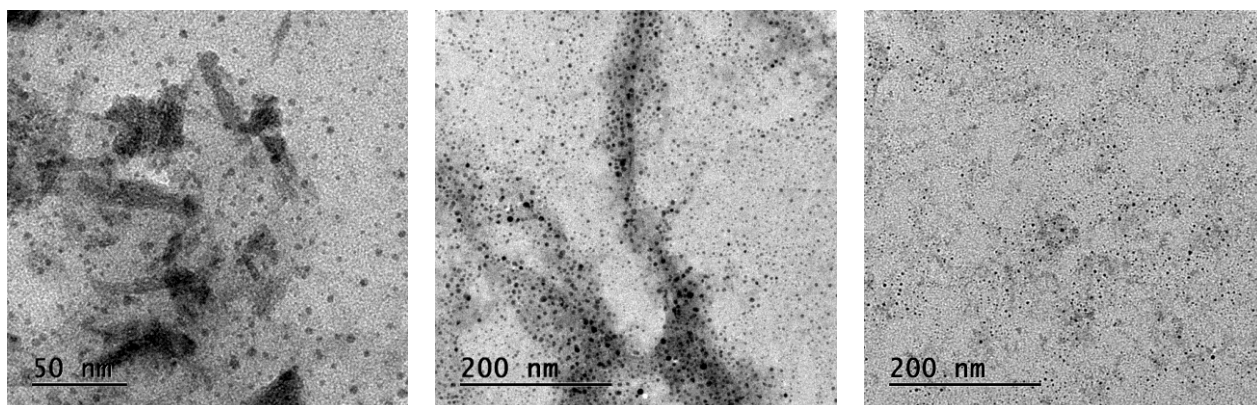


Figure S4E. TEM images of the circular objects formed by the self-assembly of compound **GC1** ($1.0 \cdot 10^{-6}$ M, H₂O pH 2) on Carbon-Cu grids.

1. F. Aparicio, P. B. Chamorro, R. Chamorro, S. Casado and D. González-Rodríguez, Nanostructured Micelle Nanotubes Self-Assembled from Dinucleobase Monomers in Water, *Angew. Chem., Int. Ed.*, 2020, DOI: 10.1002/anie.202006877.
2. E. Akiyama, M. Teduka, S. Maehama and T. Kamohara, Preparation of Polyurethanes *via* Polycondensation and their Properties, *Kobunshi Ronbunshu*, 2013, **70**, 550-558.
3. R. Lazny, A. Nodzevska and K. Wolosewicz, New Simple Polymeric Supports with Hydrazone Linkers for Solid-Phase Synthesis of Ketones and Primary Amines, *Synthesis*, 2003, **2003**, 2858-2864.
4. S. Sulzer-Mosse, C. Lamberth and P. Kubizna, Synthesis of Ring-Opened Analogues of Oxysterol-Binding Protein-Inhibiting Piperidinyl-thiazole Fungicides, *Synlett*, 2017, **28**, 2277-2280.
5. S. D. Lepore and Y. He, Use of Sonication for the Coupling of Sterically Hindered Substrates in the Phenolic Mitsunobu Reaction, *J. Org. Chem.*, 2003, **68**, 8261-8263.
6. M. A. Beuwer, M. F. Knopper, L. Albertazzi, D. van der Zwaag, W. G. Ellenbroek, E. W. Meijer, M. W. J. Prins and P. Zijlstra, Mechanical properties of single supramolecular polymers from correlative AFM and fluorescence microscopy, *Polym. Chem.*, 2016, **7**, 7260-7268.
7. H. M. M. ten Eikelder, A. J. Markvoort, T. F. A. de Greef and P. A. J. Hilbers, An Equilibrium Model for Chiral Amplification in Supramolecular Polymers, *J. Phys. Chem. B*, 2012, **116**, 5291-5301.
8. P. A. Korevaar, C. Schaefer, T. F. A. de Greef and E. W. Meijer, Controlling Chemical Self-Assembly by Solvent-Dependent Dynamics, *J. Am. Chem. Soc.*, 2012, **134**, 13482-13491.